scientific reports

Check for updates

OPEN

Analytical solutions and chaotic dynamics of the extended KP–Boussinesq model via phase diagnostics

Mehmet Şenol[1], Bahadır Kopçasız[2], Enayatullah Serat[1], Homan Emadifar[3,4]✉ & Karim K. Ahmed[5]

This study investigates the dynamical behavior of a three-dimensional extended Kadomtsev–Petviashvili–Boussinesq (eKP–BO) equation, a higher-dimensional wave system that unifies Kadomtsev–Petviashvili-type weak dispersion with Boussinesq-type bidirectional propagation. Using the $\exp(-\psi(\xi))$-expansion method, we systematically construct diverse classes of exact solutions of hyperbolic, trigonometric, and rational types. These analytical results enrich the family of admissible solitary and lump-type wave structures and provide closed-form benchmarks for validating numerical simulations. Uncover the underlying dynamics by reducing the governing equation to a planar system. This can then be analyzed through phase portraits, bifurcation diagrams, Poincaré sections, and time series. The results will reveal equilibrium structures such as centers, saddles, and cusps, as well as transitions from regular oscillations to period-doubling and fully developed chaos under period forcing. The study will also highlight both the advantages and limitations of the exponential expansion method, focusing on its ability to generate rich explicit solutions while noting its dependence on balance conditions. In sum, the results shed light on the nonlinear dispersive wave dynamics of the eKP–BO model in the unified framework and identify several potential future research paths, such as fractional-order models, stochastic perturbations, and hybrid analytical–numerical methods.

Keywords Extended Kadomtsev–Petviashvili–Boussinesq equation, $\exp(-\psi(\xi))$-expansion method, Soliton solutions, Bifurcation analysis, Chaotic dynamics, Phase portraits, Poincaré sections, Time–series analysis, Sensitivity studies, Nonlinear wave propagation

The most effective mathematical modeling tools for expressing the spatial and temporal variations of physical quantities like heat, fluid velocity, electromagnetic fields, or wave amplitudes are partial differential equations (PDEs)[1]. However, linear PDEs have long been studied and solved. At the same time, nonlinear partial differential equations (NLPDEs) are a considerably larger and more challenging family of problems that appear practically everywhere in natural applications. The PDE is deemed nonlinear if the unknown function or its derivatives manifest in a nonlinear form, such as nonlinear powers, derivative products, or nonlinear functions of the solution. This nonlinearity greatly complicates both the theoretical analysis and the numerical solution of the equations.

NLPDEs usually lack closed-form solutions and rely on sophisticated mathematical and computational tools, unlike linear PDEs, which usually permit the superposition of solutions and may be solved analytically using techniques like variable separation or Fourier transforms. Numerous scientific and engineering domains encounter NLPDEs. Viscous fluid motion in fluid dynamics is governed by the Navier-Stokes equations, which are inherently nonlinear. In general relativity, the structure of spacetime is described by Einstein's field equations, which are NLPDEs. Nonlinear wave equations describe a wide range of phenomena, from shallow water waves (by the KdV equation) to optical pulses in fiber optics (via the nonlinear Schrödinger equation)[2,3].

[1]Department of Mathematics, Nevşehir Hacı Bektaş Veli University, Nevşehir, Turkey. [2]Department of Basic Sciences, Faculty of Engineering and Architecture, Istanbul Gelisim University, Istanbul, Turkey. [3]Department of Mathematics, Saveetha School of Engineering, Saveetha Institute of Medical and Technical Sciences, Saveetha University, Chennai 602 105, Tamil Nadu, India. [4]Department of Basic Sciences, Technical and Vocational University (TVU), Tehran, Iran. [5]Department of Mathematics, Faculty of Engineering, German International University (GIU), New Administrative Capital, Cairo, Egypt. ✉email: homan_emadi@yahoo.com

More recently, much has been going on in the field of applications of enhanced analytical and numerical tools to nonlinear evolution equations, a testament to their flexibility and richness in physical connotations. In particular, Asjad et al. treated the Nizhnik–Novikov–Veselov equation and obtained exact invariant travelling-wave soliton solutions with dynamical analyses[4]. Majid et al. investigated the Riemann wave equation and indicated definite soliton structures and their sensitivity[5], while Asjad et al. performed an in-depth sensitivity analysis of solutions to the nonlinear Landau–Ginzburg–Higgs equation using the generalized projective Riccati method[6]. Related developments have also occurred in plasma and atmospheric dynamics, with Alqurashi et al. demonstrating solitary wave patterns with chaotic behavior in tropical and mid-latitude regions[7]. Also, Ullah et al. applied the Sardar-subequation method to nonlinear optical models and obtained new wave structures[8], while they illuminated the dynamics of nonlinear optics via various analytical methods[9]. All these studies collectively emphasize the increasing importance of strong solution methods and serve as a strong motivation for the present research, where the $\exp(-\psi(\xi))$-expansion method is employed to address the extended KP-Boussinesq equation. In conjunction with these developments, there have been other developments in studying nonlinear dynamical models. For example, analytical solutions of the modified Benjamin–Bona–Mahony equation were reported with applications in nonlinear optics[10]. The fractional Gross–Pitaevskii model was also investigated, in which its complex dynamical behavior and solutions were demonstrated[11]. In addition, bifurcation, multistability, and soliton dynamics in the noisy potential Korteweg–de Vries equation were explored, which exhibit the inner complexity of nonlinear evolution systems[12]. These studies further stimulate the present work and highlight the general significance of exploring exact solutions and dynamical behaviors of extended nonlinear PDEs.

The Kadomtsev-Petviashvili (KP) hierarchy is a prominent work in solitary waves theory that describes interesting higher-dimensional wave occurrences in NLPDEs. There are some excellent scientific properties and uses for the KP hierarchy. Numerous extended KP hierarchies that preserve the original KP hierarchy's integrable structures have been created and extensively examined in the literature[13].

Numerous KP Eq. (1.1) and Boussinesq (BO) Eq. (1.2) that occur in (1+1) dimensions and higher dimensions have been the subject of extensive research. To investigate the stability of the well-known Korteweg-de Vries equation in two-dimensional media, the classic KP Eq. (1.1) was developed. A vast amount of research has been done on the KP equation, which describes a wide range of physical phenomena, including fluid dynamics[14–16], dust acoustic waves, weakly nonlinear quasi-unidirectional waves[17,18], and many more. In addition, the KP equation admits a rich variety of exact solutions, each characterized by distinct structures and dynamical features.

The underlying dynamics and solution structures of the (3+1)-dimensional KP-like equations with constant coefficients are examined in this work. The $\exp(-\psi(\xi))$-expansion technique is used to derive a large number of exact wave solutions systematically. These consist of lump wave solutions and N-soliton solutions.

The following is the standard integrable KP equation[19]:

$$(\varphi_t + 6\varphi\varphi_x + \varphi_{xxx})_x + \lambda\varphi_{yy} = 0. \tag{1.1}$$

It has a weak dispersion term (φ_{xxxx}) and a quadratic nonlinearity term $(\varphi\varphi_x)_x$, admitting weakly dispersive waves. Eq. (1.1) is used in many physical contexts and describes the phenomenon of small surface tension relative to the gravitational force in fluid dynamics[20–22]. However, the BO equation says

$$\varphi_{tt} - \varphi_{xxxx} - \varphi_{xx} - 3(\varphi^2)_{xx} = 0, \tag{1.2}$$

where the height of a fluid's free surface is represented by the real-valued, sufficiently often differentiable function $\varphi(x,t)$, and partial derivatives are indicated by subscripts. Small-amplitude dispersive waves traveling in both left and right directions in shallow water are modeled by the Boussinesq Eq. (1.2)[23–26]. A great deal of research has been done to investigate a large number of exact solutions to the two well-known Eqs. (1.1) and (1.2).

Additionally, the following extended KP (eKP) equation was put out[27]:

$$(\varphi_t + 6\varphi\varphi_x + \varphi_{xxx})_x - \varphi_{yy} + \lambda\varphi_{tt} + \mu\varphi_{yt} = 0, \tag{1.3}$$

where $\varphi = \varphi(x,y,t)$ is a differentiable function, λ and μ are non-zero constants, and $\lambda\varphi_{tt}$ and $\mu\varphi_{ty}$ are added to the standard KP Eq. (1.1). The KP equation can also be extended as follows[28]:

$$(\varphi_t + 6\varphi\varphi_x + \varphi_{xxx})_x - \varphi_{yy} - \frac{\delta^2}{4}\varphi_{tt} + \delta\varphi_{ty} + \beta\varphi_{xt} = 0. \tag{1.4}$$

Finally, three extensions of (2+1)-dimensional dispersive equations are provided in Ref.[29] as:

$$\varphi_{xt} + \delta(\varphi_{xxxx} + 6\varphi_x\varphi_{xx}) + \beta\varphi_{yy} + a\varphi_{xx} + b\varphi_{xy} = 0. \tag{1.5}$$

$$\varphi_{xt} + \delta(\varphi_{xxxx} + 6\varphi_x\varphi_{xx}) + \beta\varphi_{tt} + a\varphi_{xx} + b\varphi_{xy} = 0, \tag{1.6}$$

and

$$\varphi_{xt} + \delta(\varphi_{xxxx} + 6\varphi_x\varphi_{xx}) + \beta\varphi_{yy} + \gamma\varphi_{tt} + a\varphi_{xx} + b\varphi_{xy} + c\varphi_{yt} = 0, \tag{1.7}$$

were examined, where $\delta, \beta, \gamma, a, b$, and c are arbitrary parameters and $\varphi = \varphi(x,y,t)$ is a differentiable function with respect to the spatial variables x and y and the temporal variable t.

The following three new (3+1)-dimensional equations have been proposed very recently in[30].

$$(\varphi_t + 6\varphi\varphi_x + \varphi_{xxx})_x + \lambda_1\varphi_{xx} + \lambda_2\varphi_{xy} + \lambda_3\varphi_{xz} + \delta\varphi_{yy} = 0, \tag{1.8}$$

$$(\varphi_t + 6\varphi\varphi_x + \varphi_{xxx})_x + \lambda_1\varphi_{xx} + \lambda_2\varphi_{xy} + \lambda_3\varphi_{xz} + \beta\varphi_{zz} = 0, \tag{1.9}$$

$$(\varphi_t + 6\varphi\varphi_x + \varphi_{xxx})_x + \lambda_1\varphi_{xx} + \lambda_2\varphi_{xy} + \lambda_3\varphi_{xz} + \gamma\varphi_{tt} = 0, \tag{1.10}$$

which will be called the first extended KP equation (1eKP), second extended KP equation (2eKP), and extended KP-Boussinesq equation (eKP–BO), respectively, where δ, β, γ, and $\lambda_i, (i = 1, 2, 3, \ldots)$ are non-zero parameters. Notice that the last term in each equation of (1.8)–(1.10) is the only term that changes between these equations, while the other terms in each equation remain unchanged.

This paper focuses on (3+1)-dimensional Kadomtsev–Petviashvili–Boussinesq (eKP-BO) Eq. (1.10) where t, γ, λ_i, and $i = 1, 2, 3, \ldots$ are non-zero arbitrary parameters, and $\varphi = \varphi(x, y, t)$ is a differentiable function concerning the spatial variables *x*, *y*, and *z*. It is clear that the terms $\delta\varphi_{yy}$ in Eq. (1.8) and $\beta\varphi_{zz}$ in Eq. (1.9), respectively, are replaced by the term $\gamma\varphi_{tt}$ in Eq. (1.10) as well. The conventional Boussinesq equation typically has the terms $\gamma\varphi_{tt}$, φ_{xxxx} and $\lambda_1\varphi_{xx}$ in Eq. (1.10) as well.

The extended Kadomtsev-Petviashvili–Boussinesq equation is chosen because it naturally couples the weakly dispersive character of KP-type models with the bidirectional propagation of Boussinesq-type systems. This unified structure makes it particularly relevant for describing higher-dimensional nonlinear waves in shallow-water hydrodynamics, plasma oscillations, and nonlinear optical media. While the KP and Boussinesq equations have been extensively studied in isolation, their combined extension has not previously been investigated in a comprehensive way that includes both explicit soliton solutions and qualitative dynamical analysis. For this reason, the present work provides new insight into how solitary and lump-type waveforms interact with bifurcation structures and chaotic regimes within a single modeling framework.

We construct numerous soliton solutions to demonstrate the rich analytical structure of the eKP–BO equation. In addition, a class of lump-type solutions is explored for various parameter regimes, highlighting the diversity and flexibility of exact wave structures admitted by the model. These results not only deepen the understanding of the underlying nonlinear dynamics but also serve as valuable benchmarks for validating numerical algorithms. Given their complexity and relevance, such equations are widely used in computational mathematics to test, calibrate, and verify methods for solving NLPDEs, with implications for both theoretical development and applied modeling.

To analyze such nonlinear wave models, a variety of solution techniques have been developed, including the $\tanh$-function method, Hirota bilinear formalism, and (G'/G)-expansion approaches. In this study, we adopt the $\exp(-\psi(\xi))$-expansion method because of its systematic structure and flexibility. The method is capable of producing different families of exact solutions, hyperbolic, trigonometric, and rational, within a unified framework, and the resulting expressions can be verified symbolically. These properties make it a reliable tool for constructing closed-form benchmarks that can later be used to validate numerical simulations and to interpret qualitative dynamics. A limitation of the method is that it relies on balancing the highest-order nonlinear and derivative terms, so it may not capture all possible nonlinear structures or multi-soliton interactions. Nevertheless, within its scope, it provides a direct and efficient algorithm for generating explicit solitary and lump-type solutions.

Compared with alternative approaches, the $\exp(-\psi(\xi))$-expansion method has several advantages for the present model. Unlike the $\tanh$-method, which typically yields only hyperbolic solutions, or the Hirota bilinear method, which requires a suitable bilinearization, the $\exp(-\psi(\xi))$-expansion offers a more versatile route to multiple waveform types without changing the underlying ansatz. In addition, in contrast to the (G'/G) -expansion, which can be limited in generating rational forms, the present method naturally accommodates hyperbolic, trigonometric, and rational families in one framework. This versatility aligns well with the objectives of our work, where exact solution construction is combined with qualitative bifurcation and chaos analysis of the same higher-dimensional equation.

In addition, recent studies demonstrate how chaos and stability analyses enrich diverse nonlinear systems, including advection–diffusion–reaction models, the stochastic Davey–Stewartson equation, embedded carbon nanotubes, and the Klein–Fock–Gordon equation[31–34].

The structure of the paper is as follows: the mathematical model and the $\exp(-\psi(\xi))$–expansion method are presented, also several exact analytical solutions are given in Section 2. In Section 3, graphical illustrations of the soliton solutions are offered. The bifurcation phenomena of the reduced system are discussed in Section 4 through phase portraits. Section 5 analyzes the chaotic dynamics and sensitivity of the system to external perturbations. Finally, the main findings and potential directions for future research are summarized in Section 6.

Mathematical model and analytical method

The $\exp(-\psi(\xi))$-expansion method

The $\exp(-\psi(\xi))$–expansion method is an influential analytical method for deriving exact solutions of nonlinear partial differential equations. The method relies on the postulate that the solution can be written as a finite series with respect to exponential functions in an auxiliary variable $\psi(\xi)$, where ξ is a traveling wave variable. The method reduces the original nonlinear PDE to an ordinary differential equation (ODE) through a wave transformation. The ensuing ODE is then solved by making a finite series ansatz involving $\exp(-\psi(\xi))$ and determining the coefficients by balancing the highest-order nonlinear term and the derivative term. One of the most significant features of the method is the capacity to provide different classes of solutions, including hyperbolic, trigonometric, and rational forms, based on the form of the reduced equation and the parameter

choices. Owing to the systematic algorithm and flexibility, the $\exp(-\psi(\xi))$–expansion method has been an extensively used tool for revealing exact traveling wave solutions of intricate nonlinear systems.

Let us consider the nonlinear evolution equation in the form

$$P(\varphi, \varphi_x, \varphi_y, \varphi_z, \varphi_t, \varphi_{xx}, \varphi_{xy}, \varphi_{xz}, \varphi_{xt}, ...) = 0, \tag{2.1}$$

where $\varphi = \varphi(x, y, z, t)$ is an unknown function, P is a polynomial in $\varphi(x, y, z, t)$ and its derivatives, in which the highest order derivatives and nonlinear terms are involved, and the subscripts indicate partial derivatives. In order to investigate solitary wave solutions of Eq. (2.1) by using the $\exp(-\psi(\xi))$expansion method, we have to perform the following important steps:

Step 1: We combine the real variables *x*, *y*, *z*, and *t* by a compound variable ξ

$$\xi = ax + by + cz + dt, \quad \varphi(x, y, z, t) = \psi(\xi). \tag{2.2}$$

Step 2: Eq. (1.10) is reduced to the following ordinary differential equation (ODE) when we substitute Eq. (2.1) into it:

$$\Delta(\psi(\xi), \psi'(\xi), \psi''(\xi), \ldots) = 0. \tag{2.3}$$

Step 3: A finite series can be constructed from the exact solutions:

$$\psi(\xi) = \sum_{r=0}^{N} a_r (exp(-Q(\xi)))^r, \quad a_N \neq 0, \quad 0 \leq r \leq N. \tag{2.4}$$

Step 4: $Q = Q(\xi)$ satisfies the following ODE:

$$Q'(\xi) = \mu \exp(Q(\xi)) + \exp(-Q(\xi)) + \lambda. \tag{2.5}$$

Step 5: The following are the solutions to Eq. (2.5) depending on the pertinent parameters:

$$Q(\xi) = \begin{cases} \ln\left(\frac{-\sqrt{(\lambda^2-4\mu)}\tanh(\frac{\sqrt{(\lambda^2-4\mu)}}{2}(\xi+h))-\lambda}{2\mu}\right), \ \lambda^2-4\mu>0, \ \mu\neq 0, \\ \ln\left(\frac{\sqrt{(4\mu-\lambda^2)}\tan(\frac{\sqrt{(4\mu-\lambda^2)}}{2}(\xi+h))-\lambda}{2\mu}\right), \ \lambda^2-4\mu<0, \ \mu\neq 0, \\ -\ln\left(\frac{\lambda}{\sinh(\lambda(h+\xi))+\cosh(\lambda(h+\xi))-1}\right), \ \lambda^2-4\mu>0, \ \lambda\neq 0, \ \mu=0, \\ \ln\left(-\frac{2(\lambda(\xi+h)+2)}{\lambda^2(\xi+h)}\right), \ \lambda^2-4\mu=0, \ \lambda\neq 0, \ \mu\neq 0, \\ \ln(\xi+h), \ \lambda^2-4\mu=0, \ \lambda=0, \ \mu=0. \end{cases} \tag{2.6}$$

where the integration constant is denoted by *h*.

Step 6: The positive integer N in Eq. (2.4) is computed using the homogeneous balance between the highest order derivatives of $\psi(\xi)$ and the largest nonlinear term in Eq. (2.3). By swapping out Eq. (2.4) for Eq. (2.5) and combining all terms with the same powers of exp(-ψ), the left-hand side of Eq. (2.3) becomes a polynomial. There are several algebraic equations that involve a_r $(r = 0, 1, 2, \ldots, N), c, \lambda$ and μ. Solving the system of algebraic equations yields the solutions, which are then entered into Eq. (2.4) to produce the solutions of Eq. (2.3).

Analytical solutions by $\exp(-\psi(\xi))$expansion method

The transformation (2.2) converts Eq. (1.10) into the following ODE:

$$\left(a^2\lambda_1 + ab\lambda_2 + ac\lambda_3 + ad + \gamma d^2\right)\psi(\xi) + 3a^2\psi(\xi)^2 + a^4\psi''(\xi). \tag{2.7}$$

Since $N = 2$, the series of sums obtained by substituting Eq. (2.4), looks like:

$$\psi = a_0 + a_1 \exp(-Q(\xi)) + a_2 \exp(-Q(\xi))^2. \tag{2.8}$$

When paired with Eq. (2.5), the following algebraic system of equations is created:

$$\begin{aligned}
a_1a^4\lambda\mu + 2a_2a^4\mu^2 + a_0a^2\lambda_1 + 3a_0^2a^2 + a_0ab\lambda_2 + a_0ac\lambda_3 + a_0\gamma d^2 + a_0ad &= 0,\\
6a_2a^4 + 3a_2^2a^2 &= 0,\\
10a_2a^4\lambda + 2a_1a^4 + 6a_1a_2a^2 &= 0,\\
4a_2a^4\lambda^2 + 3a_1a^4\lambda + 8a_2a^4\mu + a_2a^2\lambda_1 + 3a_1^2a^2 + 6a_0a_2a^2 + a_2ab\lambda_2 + a_2ac\lambda_3 + a_2\gamma d^2 + a_2ad &= 0,\\
a_1a^4\lambda^2 + 6a_2a^4\lambda\mu + 2a_1a^4\mu + a_1a^2\lambda_1 + 6a_0a_1a^2 + a_1ab\lambda_2 + a_1ac\lambda_3 + a_1\gamma d^2 + a_1ad &= 0.
\end{aligned}$$

For a_0, a_1, a_2, and d, we obtain one case and one set of solutions here.

Solution family:

$$a_0 = -2a^2\mu,\quad a_1 = -2a^2\lambda,\quad a_2 = -2a^2,\quad d = -\frac{\sqrt{a\left(a - 4\gamma\left(a^3\left(\lambda^2 - 4\mu\right) + a\lambda_1 + b\lambda_2 + c\lambda_3\right)\right)} + a}{2\gamma}.$$

Solution set:

For $\lambda^2 - 4\mu > 0, \mu \neq 0$,

$$\begin{aligned}
\varphi_1(x,y,z,t) = &-\frac{8a^2\mu^2}{\left(-\sqrt{\lambda^2-4\mu}\tanh\left(\frac{1}{2}\sqrt{\lambda^2-4\mu}\left(ax+by+cz-\Delta_1 t\right)\right)-\lambda\right)^2}\\
&-\frac{4a^2\lambda\mu}{-\sqrt{\lambda^2-4\mu}\tanh\left(\frac{1}{2}\sqrt{\lambda^2-4\mu}\left(ax+by+cz-\Delta_1 t\right)\right)-\lambda} - 2a^2\mu,
\end{aligned} \tag{2.9}$$

for $\lambda^2 - 4\mu < 0, \mu \neq 0$,

$$\begin{aligned}
\varphi_2(x,y,z,t) = &-\frac{8a^2\mu^2}{\left(\sqrt{4\mu-\lambda^2}\tan\left(\frac{1}{2}\sqrt{4\mu-\lambda^2}\left(ax+by+cz-\Delta_1 t\right)\right)-\lambda\right)^2}\\
&-\frac{4a^2\lambda\mu}{\sqrt{4\mu-\lambda^2}\tan\left(\frac{1}{2}\sqrt{4\mu-\lambda^2}\left(ax+by+cz-\Delta_1 t\right)\right)-\lambda} - 2a^2\mu,
\end{aligned} \tag{2.10}$$

where $\Delta_1 = \frac{1}{2\gamma}\left(\sqrt{a\left(a - 4\gamma\left(a^3\left(\lambda^2 - 4\mu\right) + a\lambda_1 + b\lambda_2 + c\lambda_3\right)\right)} + a\right)$.

For $\lambda^2 - 4\mu > 0, \lambda \neq 0$ and $\mu = 0$,

$$\begin{aligned}
\varphi_3(x,y,z,t) = &-\frac{2a^2\lambda^2}{\sinh\left(\lambda\left(ax+by+cz-\Delta_2 t\right)\right)+\cosh\left(\lambda\left(ax+by+cz-\Delta_2 t\right)\right)-1}\\
&-\frac{2a^2\lambda^2}{\left(\sinh\left(\lambda\left(ax+by+cz-\Delta_2 t\right)\right)+\cosh\left(\lambda\left(ax+by+cz-\Delta_2 t\right)\right)-1\right)^2},
\end{aligned} \tag{2.11}$$

in which, $\Delta_2 = \frac{1}{2\gamma}\left(\sqrt{a\left(a - 4\gamma\left(a^3\lambda^2 + a\lambda_1 + b\lambda_2 + c\lambda_3\right)\right)} + a\right)$.

For $\lambda^2 - 4\mu = 0, \lambda \neq 0$ and $\mu \neq 0$,

$$\varphi_4(x,y,z,t) = -\frac{a^2\lambda^4\left(ax+by+cz-\Delta_3 t\right)^2}{2\left(\lambda\left(ax+by+cz-\Delta_3 t\right)+2\right)^2} + \frac{a^2\lambda^3\left(ax+by+cz-\Delta_3 t\right)}{\lambda\left(ax+by+cz-\Delta_3 t\right)+2} - 2a^2\mu, \tag{2.12}$$

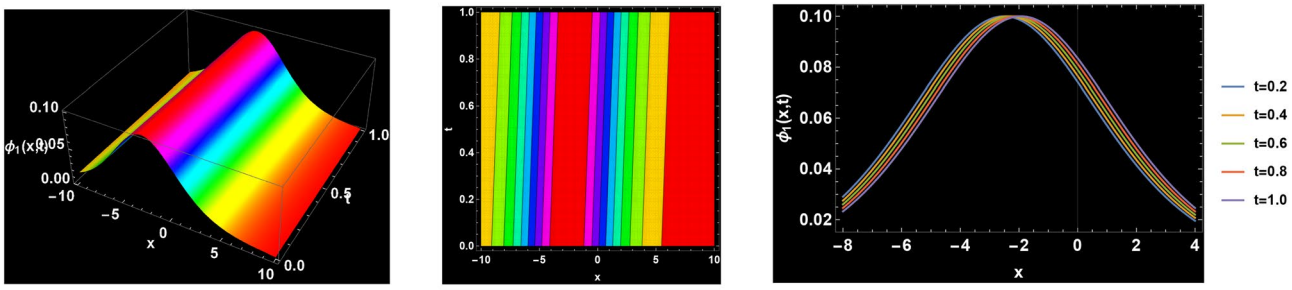
in which, $\Delta_3 = \frac{1}{2\gamma}\left(\sqrt{a\left(a - 4\gamma\left(a\lambda_1 + b\lambda_2 + c\lambda_3\right)\right)} + a\right)$.

For $\lambda^2 - 4\mu = 0, \lambda = 0$ and $\mu = 0$,

$$\varphi_5(x,y,z,t) = -\frac{2a^2}{\left(-\frac{\left(\sqrt{a(a-4\gamma(a\lambda_1+b\lambda_2+c\lambda_3))}+a\right)}{2\gamma}t + ax + by + cz\right)^2}. \tag{2.13}$$

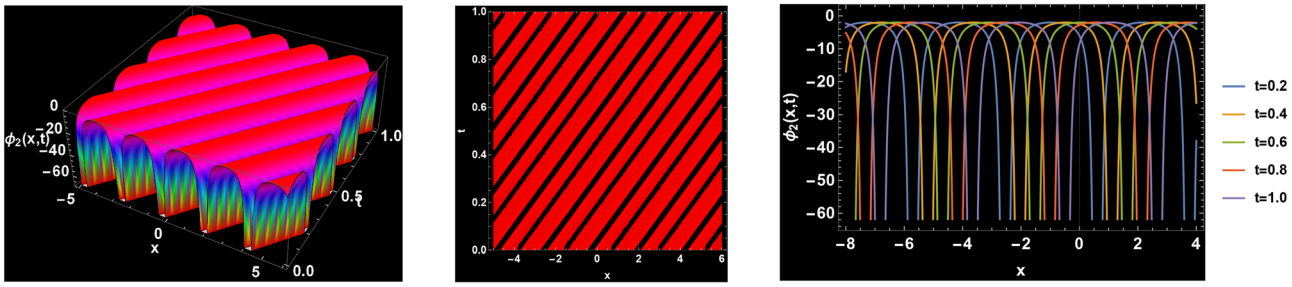
Visualization and interpretation of soliton structures

To observe the shape and dynamics of the analytical solutions derived, graphical plots are given for some cases concerning the solutions φ_1, φ_2, and φ_5. The 3D soliton profile, contour plot, and 2D projection on a temporal slice in each plot reveal the wave structures' evolution and dynamics entirely.



(a) (b) (c)

Fig. 1. (**a**) The 3D soliton, (**b**) contour and (**c**) 2D plot of φ_1 appearing in Eq. (2.9) for the values $a = 1, b = 0, c = 0, \mu = 0.2, \lambda = 1, \gamma = 1, \lambda_1 = 0, \lambda_2 = 0, \lambda_3 = 0$..



(a) (b) (c)

Fig. 2. (**a**) The 3D soliton, (**b**) contour and (**c**) 2D plot of φ_2 appearing in Eq. (2.10) for the values $y = 1, z = 1, a = 1, b = 2, c = 0.2, \mu = 2, \lambda = 0.5, \gamma = 0.2, \lambda_1 = 1, \lambda_2 = 0.5, \lambda_3 = 0.2$.

Soliton profile of φ_1

To investigate the solitary behavior of the analytical solution φ_1 given in Eq. (2.9), we present a comprehensive visual analysis based on three perspectives. Figure 1a demonstrates a three-dimensional soliton structure in the (x, t, φ) space. The solution exhibits a localized and symmetric wave profile centered around the origin. Its bell-shaped form remains intact as time evolves, indicating the robustness and preservation of its shape, which is a hallmark of classical soliton dynamics.

Figure 1b shows the contour representation of the same soliton solution. The closed and symmetric level curves in the spatial domain affirm the localized nature of the solution. Meanwhile, Fig. 1c presents time cross-sections of φ_1 at different values of t. The cross-sections exhibit the soliton's unchanged peak amplitude and spatial width over time, once again confirming the absence of dispersion or deformation. This speaks to the accuracy and stability of the resulting analytical structure achieved via the $\exp(-\psi(\xi))$-expansion method.

All the plots are obtained by choosing particular parameter values provided in the Numerical Simulations section. These selections guarantee that the argument of the square root in Eq. (2.9) is positive, providing a real-valued and physical solution. The resulting soliton profile confirms the usefulness of the obtained solution in nonlinear wave propagation models described by the eKP–BO equation.

Soliton profile of φ_2

Figure 2 displays the wave structure of the analytic solution φ_2 provided in Eq. (2.10), which is applicable for the case when $\lambda^2 - 4\mu < 0$. The solution provides a periodic-type solitary wave that is controlled by a tangent function structure, and this generates different characteristics from the profile of φ_1.

As depicted in Fig. 2a, the 3D plot records a soliton of higher amplitude and steeper gradient, which indicates a stronger nonlinear response. The more pointed peak indicates the effect of stronger nonlinear interactions for the chosen parameters. The equivalent contour plot in Fig. 2b attests to the localized nature of the soliton but with closer and denser wavefronts than φ_1.

Temporal cross-sections in Fig. 2c show a modulation of the soliton peak in time. In contrast to the steadily propagating solitary profile of φ_1, the solution φ_2 shows a "breather-like" modulation, in which the amplitude periodically changes slightly while the wave remains coherent. This is a sign of the emergence of an internal oscillation within the soliton's envelope, a signature of resonant or semi-periodic nonlinear waves.

The soliton is produced with the parameter values given in the Numerical Simulations section. These parameters give a negative $\lambda^2 - 4\mu$, guaranteeing the existence of a trigonometric soliton form and giving a visually unique waveform in the space-time domain. This validates the method's ability to create both hyperbolic and periodic soliton profiles depending on parameter regimes.

Soliton profile of φ_5

The last case to be considered, which is the analytical solution φ_5 in Eq. (2.13), is plotted in Fig. 3. This solution results when both $\lambda = 0$ and $\mu = 0$, and we get a purely rational soliton structure. In contrast to the hyperbolic and trigonometric solutions considered before, φ_5 is controlled by a decaying rational function of space and time.

Figure 3a is the 3D plot of this solution, showing the asymmetric, non-sinusoidal soliton profile without the bell shape of φ_1 or the steep oscillations of φ_2. The waveform has large tails and a tall central peak, which reflects the wider influence of dispersion. The corresponding contour plot in Fig. 3b shows a delocalized wave structure with minimal curvature, which implies slow spatial decay.

Temporal slices in Fig. 3c show that the waveform preserves its shape and undergoes weak amplitude and shape oscillations in time, revealing the equilibrium between dispersive and nonlinear effects. Compared with the other profiles, the present solution represents a more complex dynamical character, which can be attributed to multiscale structures or higher-order dispersion.

In this plot, the parameter values are assumed as in the Numerical Simulations section. Even though μ and λ explicitly vanish in the final form of the solutions, the values are retained to keep the model and the symbolic expression of the solutions consistent.

Overall, the rational soliton solution φ_5 presents a qualitatively different solitary wave behavior, enriching the diversity of possible waveforms described by the eKP–BO model and suggesting the flexibility of the method employed.

Together, these graphical observations confirm the existence and diversity of soliton solutions admitted by the investigated model. They illustrate how variations in parameter values give rise to a wide range of waveform behaviors, including stable solitary pulses, breathing-type modulations, and dispersive wave phenomena, thereby enriching the overall solution space.

Beyond the soliton structures, the eKP–BO equation also exhibits complex dynamical features when analyzed via its reduced planar form. The subsequent section delves into the system's qualitative dynamics and bifurcation properties using established tools from nonlinear dynamical systems theory.

Bifurcation analysis of the reduced dynamical system

Derivation of the reduced system

Bifurcation analysis aids in determining whether or not the underlying dynamical system depends on the values of the involved parameters. The Galilean transformation[35,36] applied to Eq. (2.2) yields the following planar dynamical system:

$$\begin{cases} \dfrac{d\psi}{d\xi} = \Omega, \\ \dfrac{d\Omega}{d\xi} = w_1\psi + w_2\psi^2, \end{cases} \tag{4.1}$$

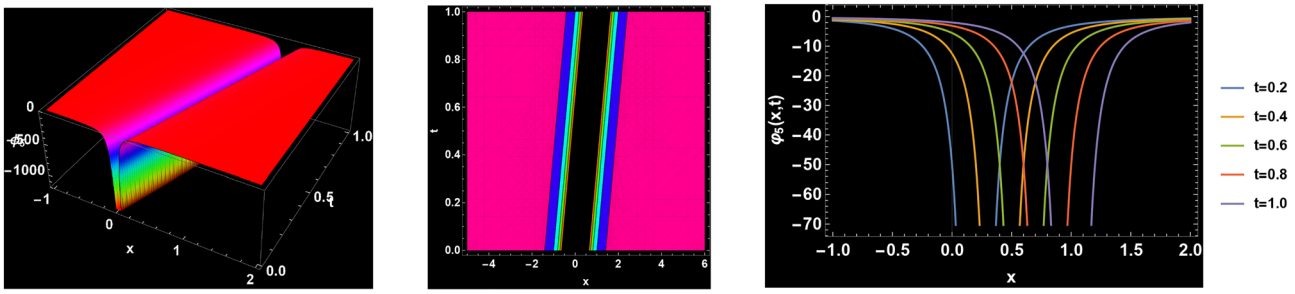
where $w_1 = -\frac{a^2\lambda_1 + ab\lambda_2 + ac\lambda_3 + ad + \gamma d^2}{a^4}$ and $w_2 = -\frac{3}{a^2}$.

The Hamiltonian is given by:

$$S(\psi, \Omega) = \frac{\Omega^2}{2} + w_1\frac{\psi^2}{2} + w_2\frac{\psi^3}{3} = s, \tag{4.2}$$

in which the Hamiltonian constant is denoted by s. The bifurcations of the system (4.1) phase portraits throughout the parameter space of w_1 and w_2 will now be investigated. The following results can be seen through qualitative analysis.

Bifurcation analysis is the linchpin in determining how qualitative behavior in the low-dimensional dynamical system emerges through variation of parameters. Bifurcation analysis informs how a transition from periodic



(a) (b) (c)

Fig. 3. (**a**) The 3D soliton, (**b**) contour and (**c**) 2D plot of φ_5 appearing in Eq. (2.13) for the values $a = 1$, $b = 0$, $c = 0$, $\mu = 0.2$, $\lambda = 1$, $\gamma = 1$, $\lambda_1 = 0$, $\lambda_2 = 0$, $\lambda_3 = 0$.

to chaotic motion takes place through the identification of changes in equilibria structures and stability. In the context of the eKP-BO model, it allows us to connect the existence of exact solitary wave solutions with the onset of more complex nonlinear dynamics in the truncated system. That is, bifurcation diagrams characterize routes such as period-doubling and characterize critical parameter thresholds at which solitary waves lose stability, hence illuminating the connection between analytical solutions and chaos.

Equilibrium points and Jacobian analysis

The first thing to note is that system (4.1) has two equilibrium points, which are as follows:

$$\mathcal{G}_1 = (0,0) \quad \text{and} \quad \mathcal{G}_2 = \left(\frac{-w_1}{w_2}, 0\right).$$

The Jacobian of (4.1) will be:

$$J(\psi,\Omega) = \det \begin{vmatrix} 0 & 1 \\ w_1 + 2w_2\psi & 0 \end{vmatrix} = -w_1 - 2w_2\psi.$$

Therefore, with regard to $J(\psi,\Omega) < 0$, the pair (ψ,Ω) can be designated as the saddle point. Additionally, it would be a cuspidal for $J(\psi,\Omega) = 0$ and the center for $J(\psi,\Omega) > 0$. By altering the parameter ranges, the intended outcomes can be obtained.

Phase portraits under parameter variations

Case 1: $w_1 > 0, \quad w_2 > 0$

For the system (4.1), represented as $\mathcal{G}_1 = (0,0)$ and $\mathcal{G}_2 = (-1,0)$, as indicated in Fig. 4a, we have successfully identified two stable points of equilibrium using the values $w_1 = 1$ and $w_2 = 1$. Both the center point characteristic of $\mathcal{G}_2$ and the saddle point characteristic of $\mathcal{G}_1$ are readily apparent.

Case 2: $w_1 > 0, \quad w_2 < 0$

The system (4.1) has two critical points for values of $w_1 = 1$ and $w_2 = -1$, namely $\mathcal{G}_1 = (0,0)$ and $\mathcal{G}_2 = (1,0)$, as shown in Fig. 4b. When we look more closely, we can see that $\mathcal{G}_1$ is a saddle point, while $\mathcal{G}_2$ is the center.

Case 3: $w_1 < 0, \quad w_2 < 0$

We have successfully extracted the equilibrium points $\mathcal{G}_1 = (0,0)$ and $\mathcal{G}_2 = (-1,0)$ from the system (4.1) shown in Fig. 4c by using the values $w_1 = -1$ and $w_2 = -1$. It is clear by looking at the phase portrait that $\mathcal{G}_1$ behaves like a center point, while $\mathcal{G}_2$ takes on the traits of a saddle.

Case 4: $w_1 < 0, \quad w_2 > 0$

The system (4.1) shows two equilibrium points for the values $w_1 = -1$ and $w_2 = 1$, namely $\mathcal{G}_1 = (0,0)$ and $\mathcal{G}_2 = (1,0)$, as shown in Fig. 4d. $\mathcal{G}_1$ is clearly a center point, and $\mathcal{G}_2$ is clearly the saddle.

Case 5: $w_1 = 0, \quad w_2 \neq 0$

Only a single point of equilibrium, $\mathcal{G}_1 = (0,0)$, can be discovered for $w_1 = 0$ and $w_2 = -1$, as shown in the example in Fig. 4e. By analyzing the Jacobian, it has been established that $\mathcal{G}_1$ behaves in a cusp manner.

For clarity in the phase portraits, we use the abbreviations **S** for saddle, **C** for center, and **D** for cusp to indicate the nature of the equilibrium points.

The phase portrait analysis reveals how the system's fixed points and stability evolve with changing parameters. To explore the system's response to external periodic perturbations, we now extend our analysis to include chaotic dynamics and sensitivity studies.

Chaotic dynamics and sensitivity analysis

Perturbed dynamical system model

Using the previously mentioned planar dynamical system in Eq. (2.2), we add the perturbation term $f_0\cos(R)$ to investigate the disordered resolution of Eq. (2.2). Thus, we obtain:

$$\begin{cases} \dfrac{d\psi}{d\xi} = \Omega, \\ \dfrac{d\Omega}{d\xi} = w_1\psi + w_2\psi^2 + f_0\cos(R), \\ \dfrac{dR}{d\xi} = \delta, \end{cases} \tag{5.1}$$

where $R = \delta\xi$. The amplitude and frequency of the external force applied to the system (5.1) are represented by the parameters f_0 and δ in the given system. In the present work, we investigate the effect of the perturbation parameters $f_0\cos(R)$ on the planar dynamical system (5.1). The influence of outside factors may lead a system to act in a random and unpredictable manner. We found this specific phenomenon in system (5.1), which is chaotic in movement in our work, whose trajectories change over time and exhibit divergences from regular patterns.

There are other methods for detecting chaos; however, in this academic paper, we will focus on the most useful ones:

- Bifurcation diagrams,
- Sensitivity to Frequency and Amplitude,

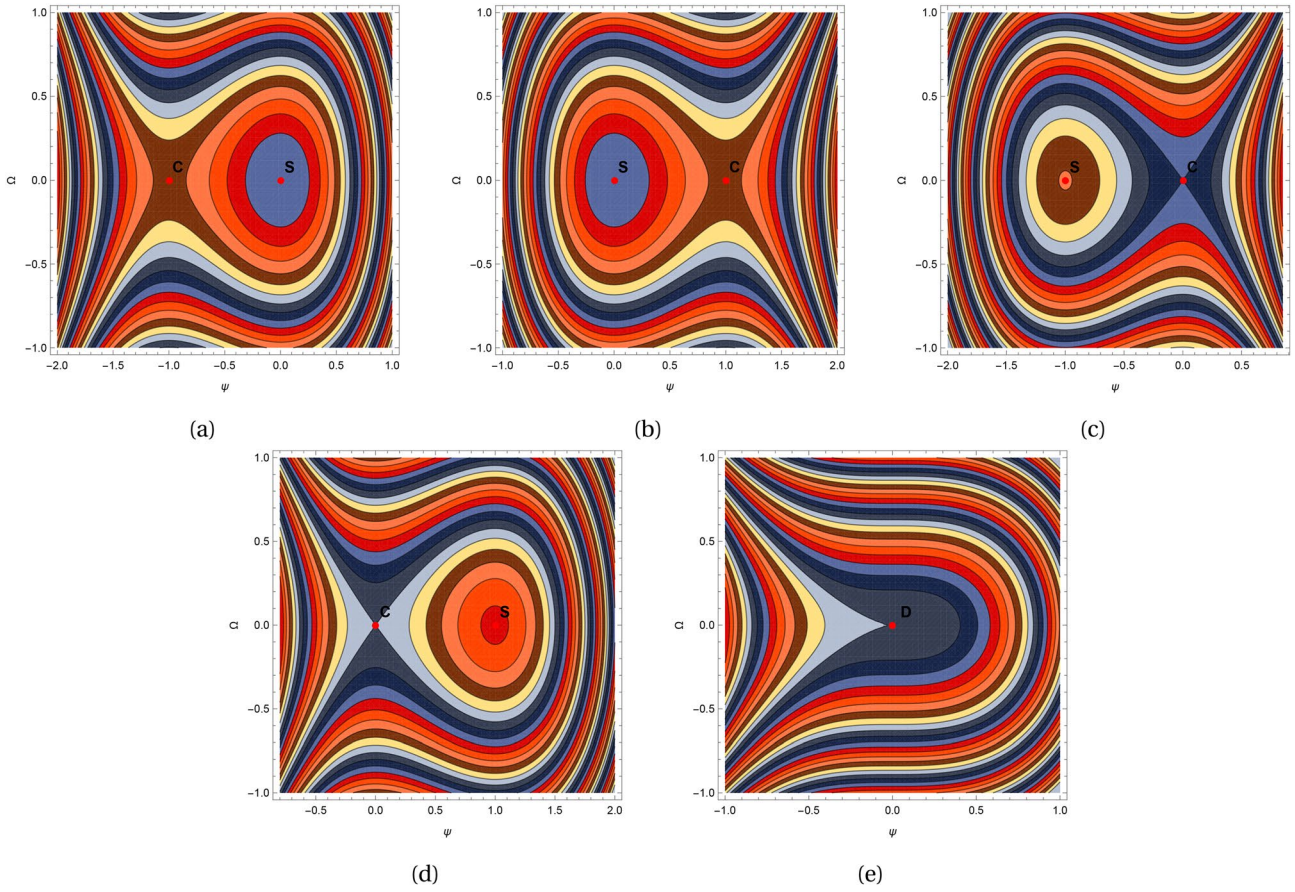


Fig. 4. Phase portraits of the reduced system (4.1) using the values (**a**) $a = i\sqrt{3}, b = i\sqrt{3}, c = i\sqrt{3}, d = 0, \lambda_1 = 1, \lambda_2 = 1, \lambda_3 = 1, \gamma = 0, w_1 = 1,$ $w_2 = 1$, (**b**) $a = \sqrt{3}, b = \sqrt{3}, c = \sqrt{3}, d = 0, \lambda_1 = -1, \lambda_2 = -1, \lambda_3 = -1, \gamma = 0, w_1 = 1,$ $w_2 = -1$, (**c**) $a = \sqrt{3}, b = \sqrt{3}, c = \sqrt{3}, d = 0, \lambda_1 = 1, \lambda_2 = 1, \lambda_3 = 1, \gamma = 0, w_1 = -1, w_2 = -1,$ (**d**) $a = i\sqrt{3}, b = i\sqrt{3}, c = i\sqrt{3}, d = 0, \lambda_1 = -1, \lambda_2 = -1, \lambda_3 = -1, \gamma = 0, w_1 = -1, w_2 = 1,$ (**e**) $a = i\sqrt{3}, b = i\sqrt{3}, c = i\sqrt{3}, d = 0, \lambda_1 = -, \lambda_2 = -0.5, \lambda_3 = -0.5, \gamma = 0, w_1 = 0, w_2 = 1$ with S (saddle), C (center), and D (cusp).

- Phase portraits,
- Poincaré map,
- Time series.

Bifurcation diagram

This scenario corresponds to the classical period–doubling route to chaos observed in many nonlinear oscillators. Importantly, the scattered branches at larger f_0 values reflect the loss of coherence in solitary wave profiles, showing how external forcing destabilizes initially regular soliton structures into irregular and turbulent-like dynamics. Hence, Fig. 5 not only illustrates the mathematical transition from order to chaos but also captures the physical thresholds at which wave stability breaks down in the extended KP–Boussinesq model.

Bifurcation analysis is a valuable method for the study of how the qualitative dynamics of nonlinear systems change with system parameters. For the considered model, Fig. 5 is a bifurcation diagram showing how the system dynamics depend on the bifurcation parameter f_0. At a small f_0, the system has regular periodic oscillations indicated by a single and distinct branch. As the f_0 is increased, a sequence of period-doubling bifurcations occurs that eventually gives rise to chaotic dynamics with densely populated and unorganized branches. This is typical of sensitive dependence on initial conditions, another hallmark of chaotic systems. The bifurcations translate physically into sensational changes in wave dynamics wherein originally stable solitary wave profiles are rendered into turbulent-like disordered forms with parametric variation. Such behavior is of vital significance in fluid mechanics, plasma physics, and nonlinear optics, where minute changes in system structure or external disturbances can trigger complex wave interactions, energy redistribution, or modulational instability. The bifurcation diagram not only identifies thresholds of dynamical transition but also provides a clue to how nonlinear wave systems can transition between order and chaos, vital to the comprehension, control, or prediction of nonlinear physical processes.

It is important to emphasize that bifurcation and chaotic analysis are complementary, even when performed under the same parameter conditions. Bifurcation diagrams show how the qualitative solution structure

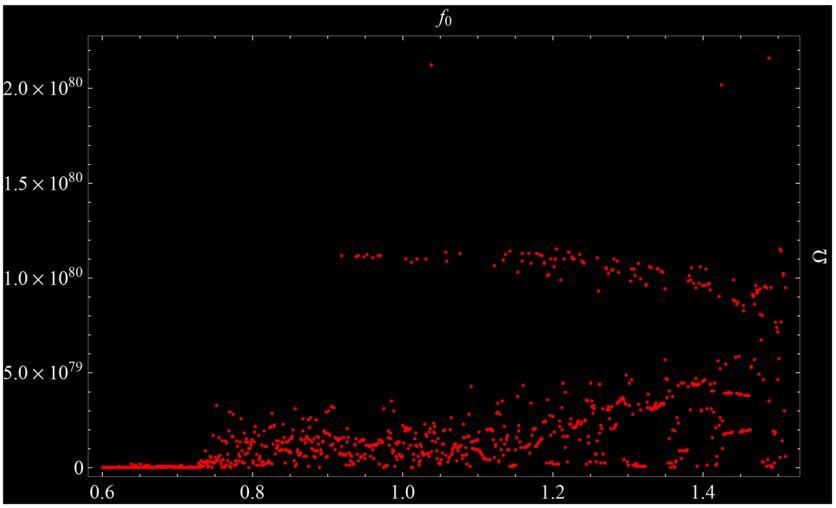


Fig. 5. Bifurcation diagram of the perturbed system (5.1) using the values $a = i\sqrt{2}$, $b = i\sqrt{2}$, $\lambda_1 = -2$, $\lambda_2 = -2$, $\lambda_3 = -1$, $\gamma = 0$, $w_1 = -2.5$,$w_2 = 1.5$, $\delta = 1.15$ with the initial condition $(\psi(0), \Omega(0)) = (0.5, 0.1)$.

is altered when system parameters are varied, such as transitions from periodic to quasi-periodic or chaotic regimes. Chaotic analysis, on the other hand, provides a deeper confirmation of the irregular dynamics of the chaotic regime itself, by its study of sensitivity to initial conditions, strange attractor geometries, and Poincaré sections. Bifurcation analysis, therefore, establishes the onset of instability and routes to chaos, while chaotic analysis confirms and characterizes the resulting chaotic behavior. This two-pronged strategy is well grounded in nonlinear dynamics[37,38], and the employment of both perspectives ensures a comprehensive understanding of the complex dynamics of the model.

Sensitivity to frequency and amplitude

Figures 6 and 7 illustrate the sensitivity of the considered system to changes of external periodic forcing amplitude (f_0) and frequency (δ). As the forcing amplitude f_0 increases (Fig. 6), the system goes from regular oscillatory to more irregular and chaotic behavior, showing that small changes in external excitation can drastically influence the course of the system. Consequently, oscillations in the frequency δ (Fig. 7) are met with a variety of dynamical behaviors, including quasi-periodic oscillations and fully developed chaos. Such sensitivity is typical for nonlinear systems perturbed and is indicative of the delicate balance between internal and external effects. Physically, the results imply that wave propagation in such media can exhibit very variable amplitude and phase transitions to parametric or environmental perturbations. Such sensitivity has immediate implications in fields such as nonlinear optics, fluid flow, and geophysical wave propagation, in which waveform control is typically problematic but needs to be precise for prediction or avoidance of instability.

Sensitivity analysis is essential in this context, as it confirms the chaotic nature of the system: even a small deviation in the initial state produces significantly different trajectories over time, a hallmark of chaos. The corresponding results are presented in Figs. 6 and 7.

Chaotic analysis (2D and 3D)

The 2D and 3D phase portraits in Figs. 8, 9, 10 and 11 provide a general view of the dynamical structure of the model. The 2D portraits (Figs. 8 and 9) illustrate the evolution of trajectories in the (ψ, Ω) plane for various values of the forcing parameters f_0 and δ. At lower values of these parameters, closed orbits and regular trajectories dominate, indicating quasi-periodic or bounded oscillations. As parameters grow, the phase space becomes densely filled with chaotic orbits, which signifies the onset of chaotic dynamics. The 3D portraits (Figs. 10 and 11) add the time dimension to this picture, showing complex attractor geometries and spiral-like flows that capture the long-time dynamics of the system. Such phase space representations are instrumental in identifying the transition to chaos as well as in understanding the stability of wave patterns. These portraits carry over to physical systems, such as optical waveguides or shallow water systems, where they describe the dynamics of propagation of wave packets or pulses under perturbations, depicting how nonlinearity and external driving can lead to intricate, usually erratic, spatiotemporal dynamics.

Although phase portraits provide continuous information about the structure of the system's orbits, they become messy in chaotic regimes. To prevent this and achieve cleaner patterns, we now turn to the Poincaré map, a discrete sampling method providing a clearer picture of the long-term dynamics.

Poincaré map

The Poincaré maps in Figs. 12 and 13 offer a very powerful tool for investigating the long-term dynamics of the system. Unlike continuous phase portraits, discrete maps sample the system's state at periodic intervals, which reduces the dimensionality and causes latent structure in the dynamics to become apparent. At lower

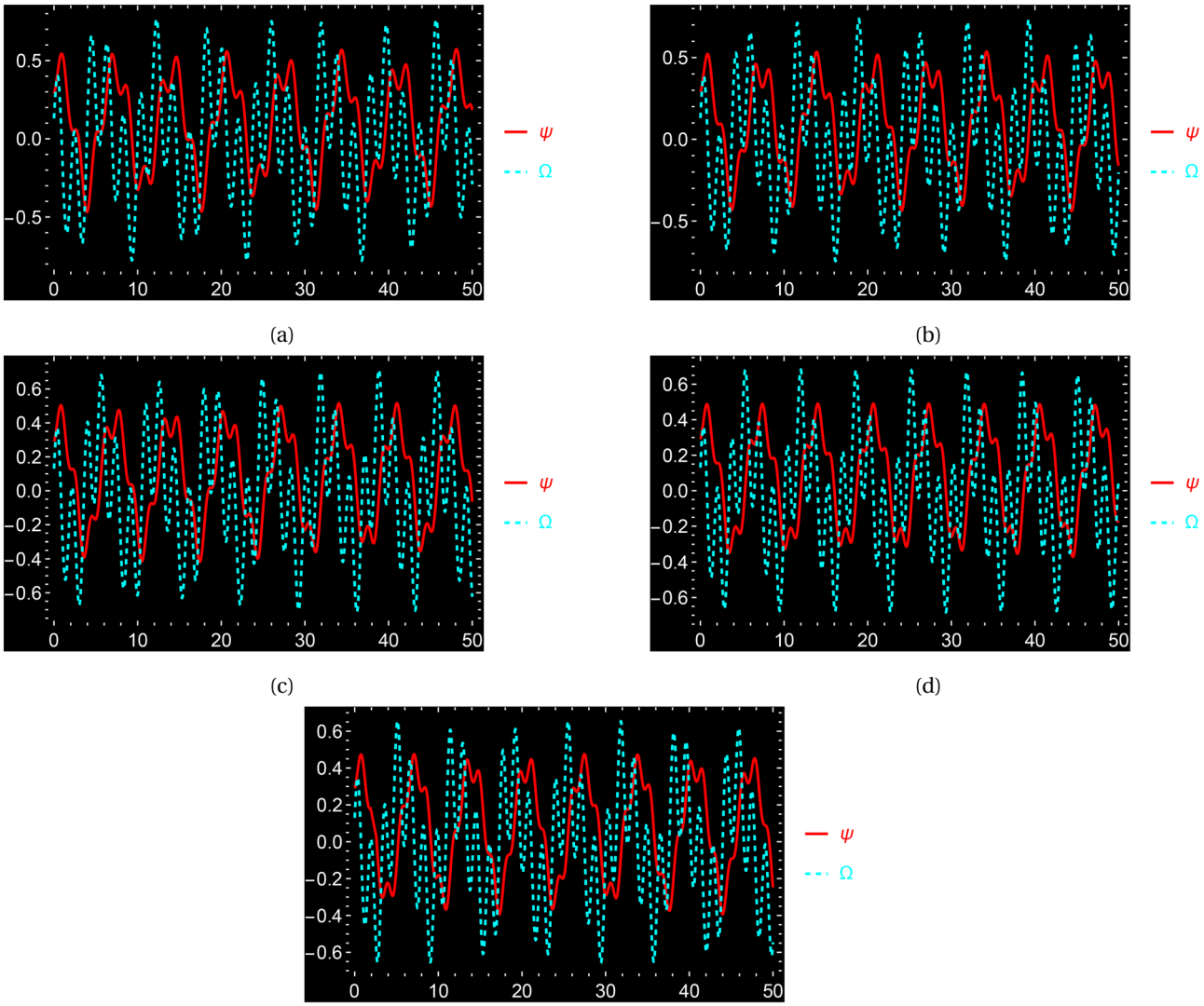


Fig. 6. Sensitivity analysis of the perturbed system (5.1) using the values $a = i\sqrt{3}, b = i\sqrt{3}, c = i\sqrt{3}, d = 0$, $\lambda_1 = -1, \lambda_2 = -1, \lambda_3 = -1, \gamma = 0, w_1 = -1, w_2 = 1, \omega = 1.20$ and (**a**) $\delta = 3.20$, (**b**) $\delta = 3.40$, (**c**) $\delta = 3.60$, (**d**) $\delta = 3.80$, (**e**) $\delta = 4$ with the initial condition $(\psi(0), \Omega(0)) = (0.29, 0.13)$.

values of the forcing parameters f_0 and δ, the Poincaré sections consist of isolated points or closed curves characteristic of periodic and quasi-periodic behavior. As the parameters are increased, these regular structures give way to scattered and dense clouds of points, indicating chaotic behavior. Such transitions are important physical indicators of instability in wave propagation systems. In physical systems, such maps correspond to periodic states of wave packets or modulated pulses in cyclic driving, providing a hint of whether the system will reproduce itself or diverge into chaos. The Poincaré map thus reinforces and complements the bifurcation and phase space analysis by graphically confirming the presence and nature of chaotic attractors.

Time series

The time series plots in Figs. 14 and 15 give a temporal view of the dynamical evolution of the system. The plots show the evolution of the state variables ψ and T with time for different values of the perturbation frequency δ and amplitude f_0. For lower δ and f_0 values, the time series exhibit smooth and regular oscillations, characteristic of stable periodic or quasi-periodic behavior. However, as these parameters are raised, the time series grow increasingly irregular, with erratic fluctuations and lack of periodicity, clear hallmarks of chaotic dynamics. This response highlights the system's ultra sensitivity to external driving forces. Physically, our results identify the destabilizing influence of the amplitude and frequency of external forcing on otherwise coherent wave structures, creating complex temporal patterns such as energy spreading, pulse splitting, or modulation instability. Time series analysis thus completes the bifurcation, phase portrait, and Poincaré map findings by confirming the onset of chaos from the point of view of time evolution that is required to predict the system's behavior in practical, time-dependent circumstances.

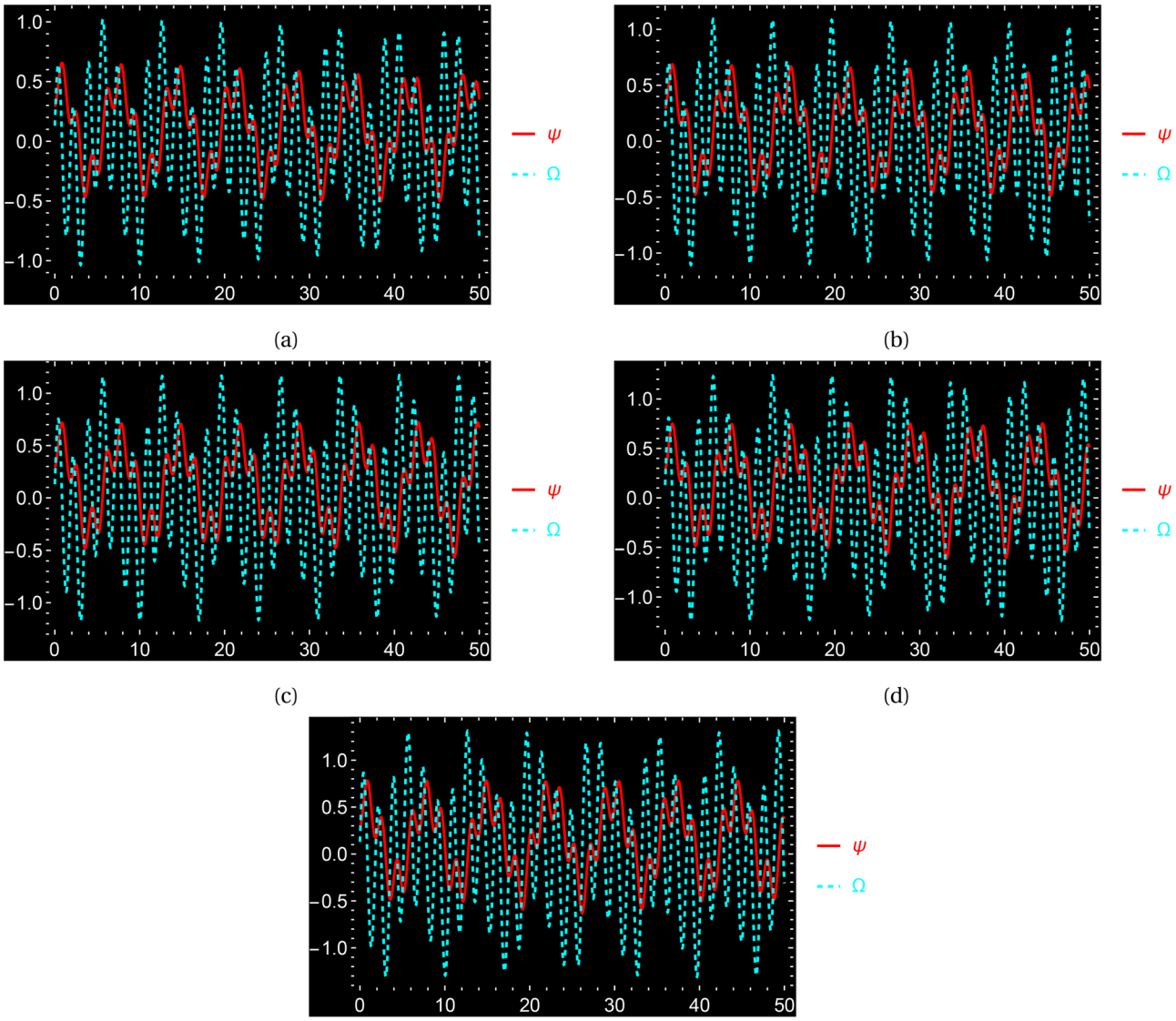


Fig. 7. Sensitivity analysis of the perturbed system (5.1) using the values $a = i\sqrt{3}, b = i\sqrt{3}, c = i\sqrt{3}, d = 0$, $\lambda_1 = -1, \lambda_2 = -1, \lambda_3 = -1, \gamma = 0, w_1 = -1, w_2 = 1, \delta = 3.60$ and (**a**) $\omega = 2.20$, (**b**) $\omega = 2.40$, (**c**) $\omega = 2.60$, (**d**) $\omega = 2.80$, (**e**) $\omega = 3.00$ with the initial condition $(\psi(0), \Omega(0)) = (0.29, 0.13)$.

Conclusion

In this paper, an extensive examination of the $(3+1)$-dimensional extended Kadomtsev–Petviashvili–Boussinesq (eKP–BO) equation, a model chosen for its ability to merge Kadomtsev–Petviashvili-type systems' weak dispersion with bidirectional propagation of Boussinesq-type dynamics, thereby providing a natural context for describing nonlinear shallow-water hydrodynamics, plasma oscillations, and nonlinear optics phenomena, was presented. By the $\exp(-\psi(\xi))$-expansion method, we derived systematically explicit traveling-wave solutions of hyperbolic, trigonometric, and rational forms, which further extend the collection of valid solitary and lump-type profiles and offer closed-form reference solutions to check numerical simulations. The method has definite strengths over more traditional techniques such as the $\tanh$-function method, the Hirota bilinear approach, and the (G'/G)-expansion procedure, in that it is able to generate multiple families of waveforms within one algorithmic framework, and the solutions so generated can be symbolically checked. It has the disadvantage of requiring balance conditions, though, and so will not pick up all multi-soliton interactions or other more exotic nonlinear states. In addition to solution construction, we reduced the equation to a two-dimensional dynamical system and performed qualitative analysis, which revealed centers, saddles, cusps, and heteroclinic orbits together with regular oscillation to chaotic dynamics upon parametric forcing. These transitions were described in terms of bifurcation diagrams, sensitivity analyses, phase portraits, Poincaré maps, and time series, all exemplifying the coexistence of coherent soliton dynamics with chaotic irregular regimes within a single mathematical model. The findings highlight not only the analytical complexity of the eKP–BO equation but

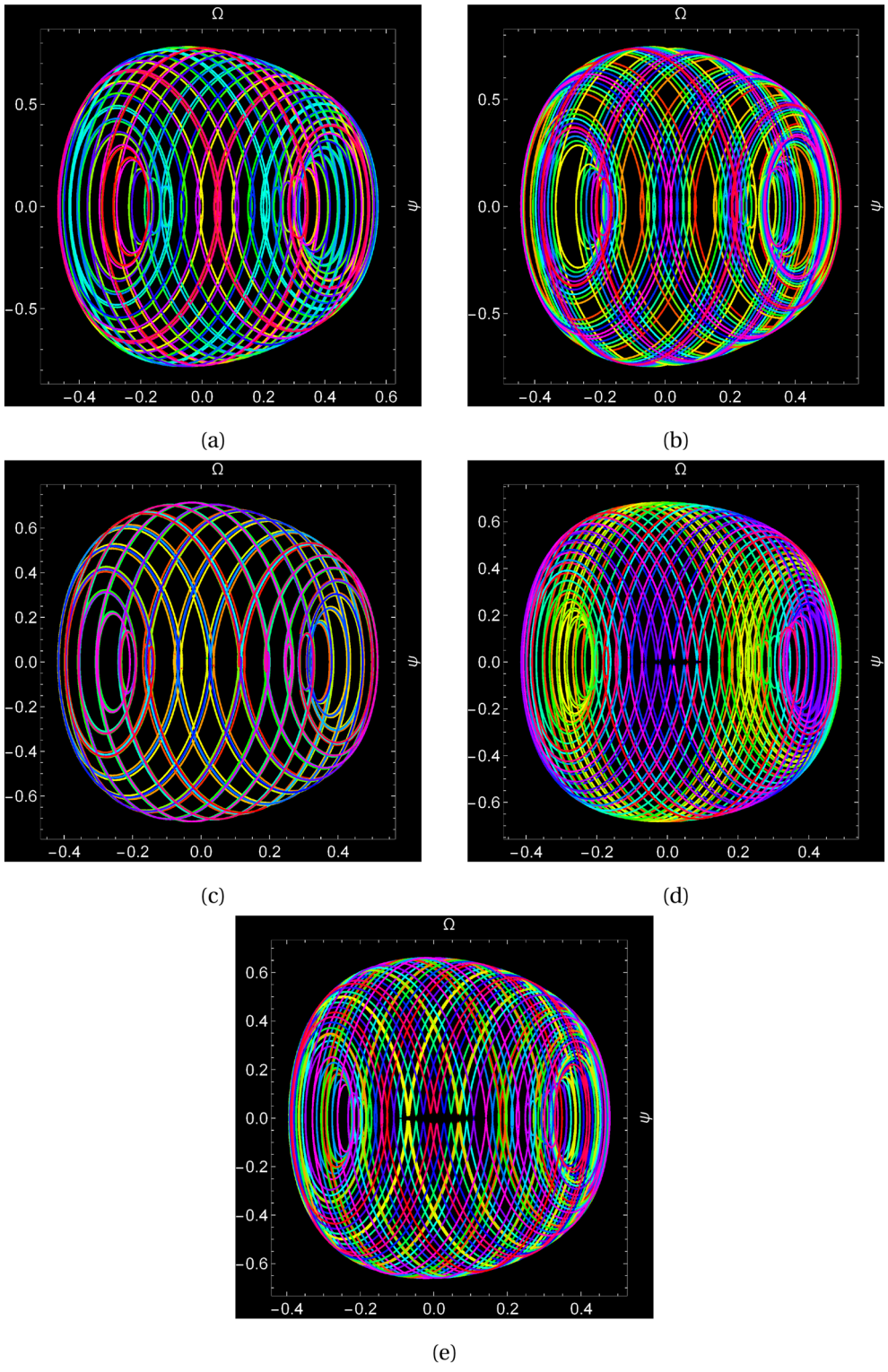


Fig. 8. 2D chaotic analysis of the perturbed system (5.1) using the values $a = i\sqrt{3}, b = i\sqrt{3}, c = i\sqrt{3}, d = 0$, $\lambda_1 = -1, \lambda_2 = -1, \lambda_3 = -1, \gamma = 0, w_1 = -1, w_2 = 1, \omega = 1.20$ and (**a**) $\delta = 3.20$, (**b**) $\delta = 3.40$, (**c**) $\delta = 3.60$, (**d**) $\delta = 3.80$, (**e**) $\delta = 4$ with the initial condition $(\psi(0), \Omega(0)) = (0.29, 0.13)$.

also the utility of combining exact solutions with dynamical systems theory in accurately describing the full range of nonlinear behaviors. Prospects on the horizon involve extension to fractional-order derivatives in order to be able to include memory effects, incorporating stochastic or dissipative perturbations to model realistic environment conditions, and application of hybrid analytical-numerical approaches like RPSM–PINN in order to advance applicability and to bridge exact solutions with simulations for the entire $(3 + 1)$-dimensional system.

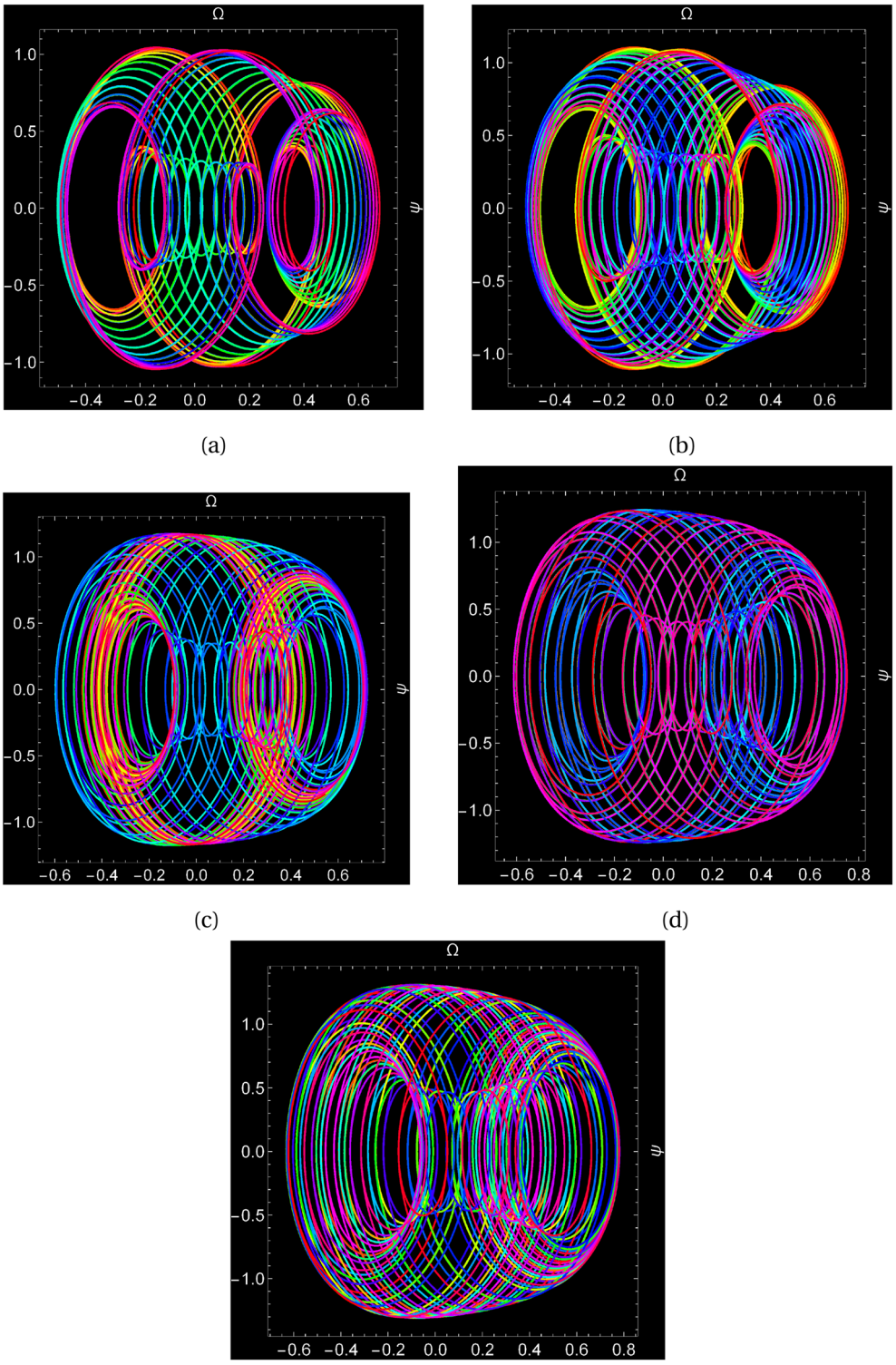


Fig. 9. 2D chaotic analysis of the perturbed system (5.1) using the values $a = i\sqrt{3}, b = i\sqrt{3}, c = i\sqrt{3}, d = 0$, $\lambda_1 = -1, \lambda_2 = -1, \lambda_3 = -1, \gamma = 0, w_1 = -1, w_2 = 1, \delta = 3.60$ and (**a**) $\omega = 2.20$, (**b**) $\omega = 2.40$, (**c**) $\omega = 2.60$, (**d**) $\omega = 2.80$, (**e**) $\omega = 3.00$ with the initial condition $(\psi(0), \Omega(0)) = (0.29, 0.13)$.

In summary, the current study sets the eKP–BO equation on a fertile basis to explore nonlinear dispersive wave dynamics and deciphers the power and limitations of the $\exp(-\phi(\xi))$-expansion technique in advancing theory and numerical simulation of complex wave behaviors.

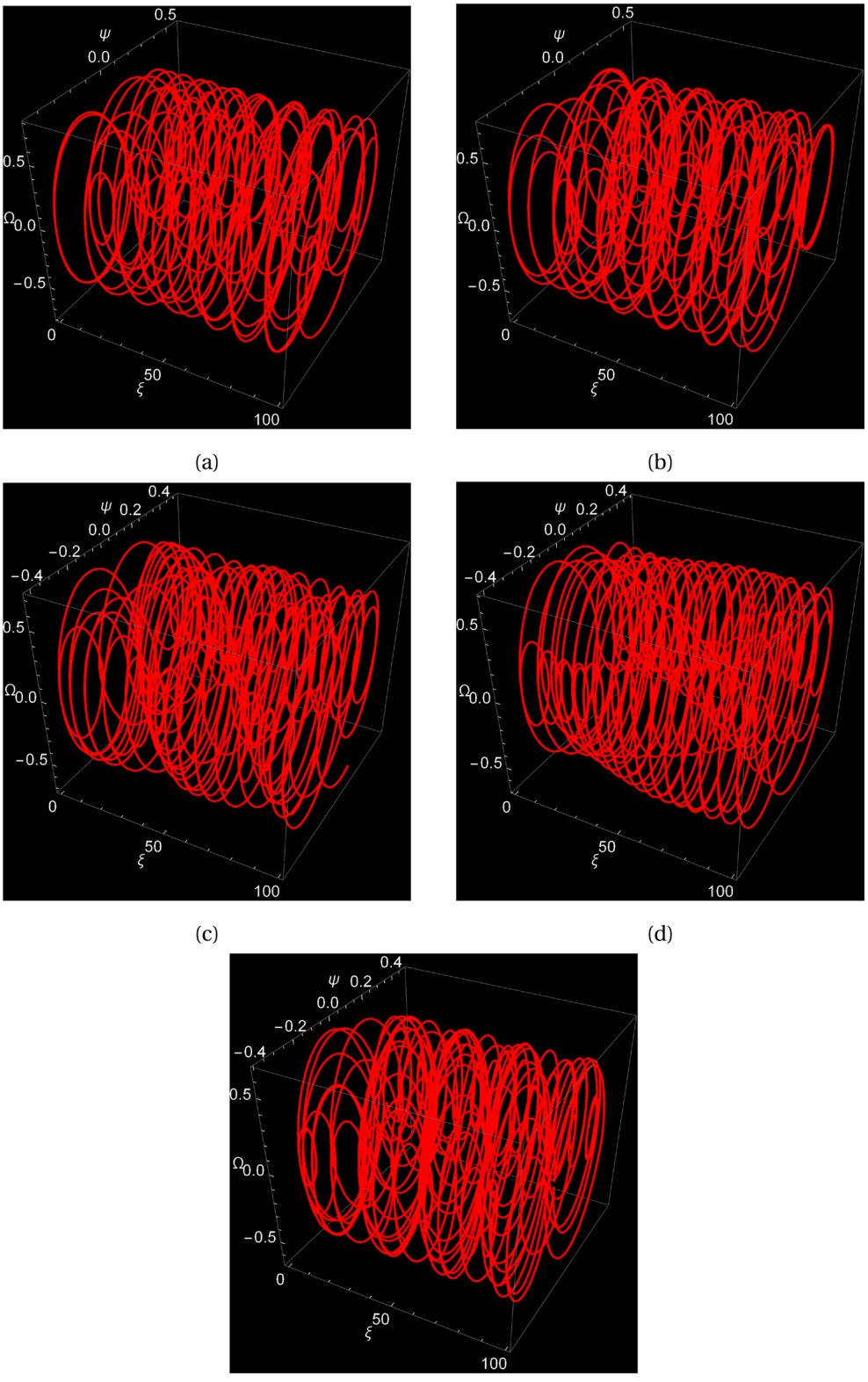


Fig. 10. 3D chaotic analysis of the perturbed system (5.1) using the values $a = i\sqrt{3}$, $b = i\sqrt{3}$, $c = i\sqrt{3}$, $d = 0$, $\lambda_1 = -1$, $\lambda_2 = -1$, $\lambda_3 = -1$, $\gamma = 0$, $w_1 = -1$, $w_2 = 1$, $\omega = 1.20$ and (**a**) $\delta = 3.20$, (**b**) $\delta = 3.40$, (**c**) $\delta = 3.60$, (**d**) $\delta = 3.80$, (**e**) $\delta = 4$ with the initial condition $(\psi(0), \Omega(0)) = (0.29, 0.13)$.

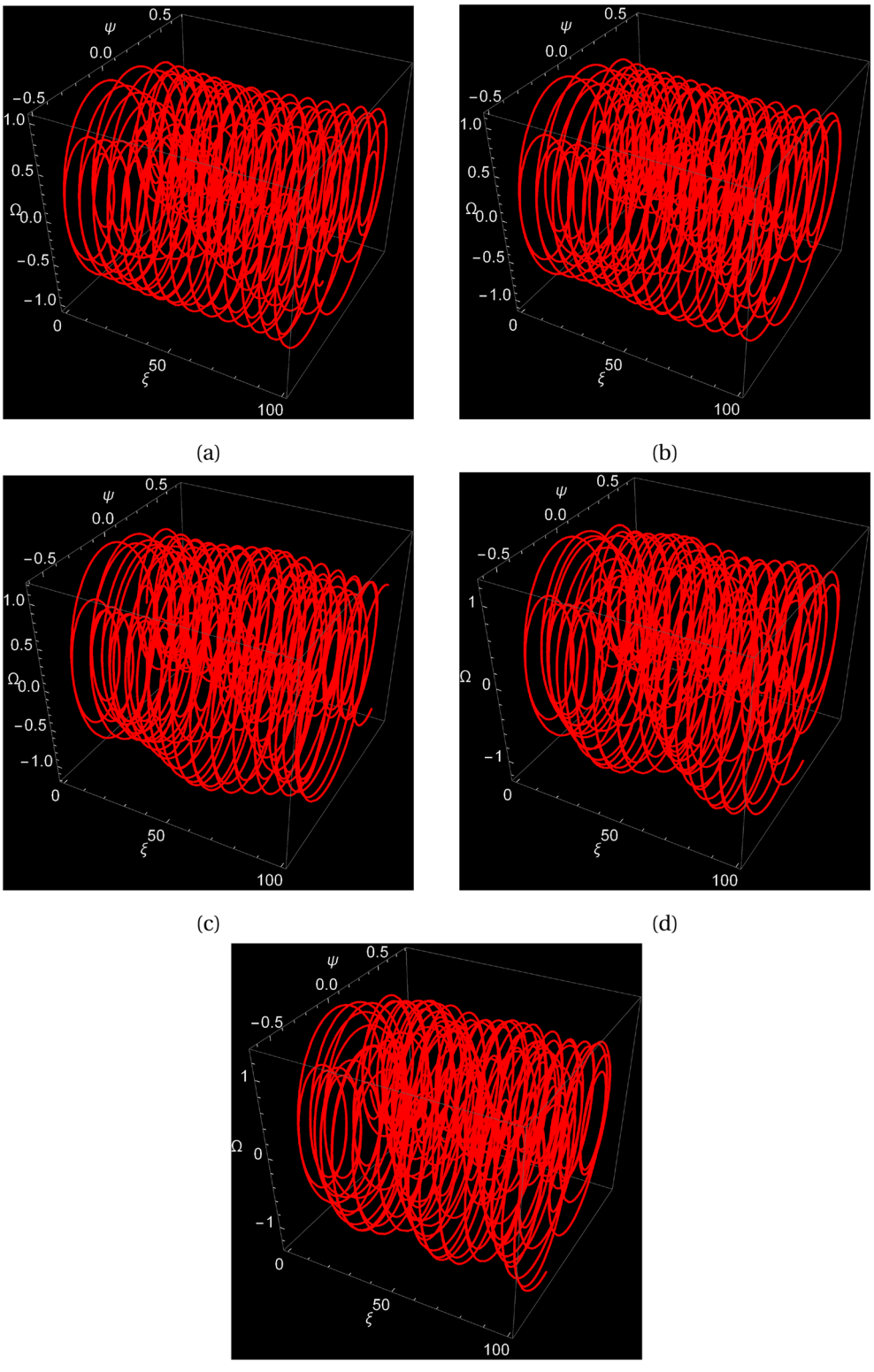


Fig. 11. 3D chaotic analysis of the perturbed system (5.1) using the values $a = i\sqrt{3}$, $b = i\sqrt{3}$, $c = i\sqrt{3}$, $d = 0$, $\lambda_1 = -1$, $\lambda_2 = -1$, $\lambda_3 = -1$, $\gamma = 0$, $w_1 = -1$, $w_2 = 1$, $\delta = 3.60$ and (**a**) $\omega = 2.20$, (**b**) $\omega = 2.40$, (**c**) $\omega = 2.60$, (**d**) $\omega = 2.80$, (**e**) $\omega = 3.00$ with the initial condition $(\psi(0), \Omega(0)) = (0.29, 0.13)$.

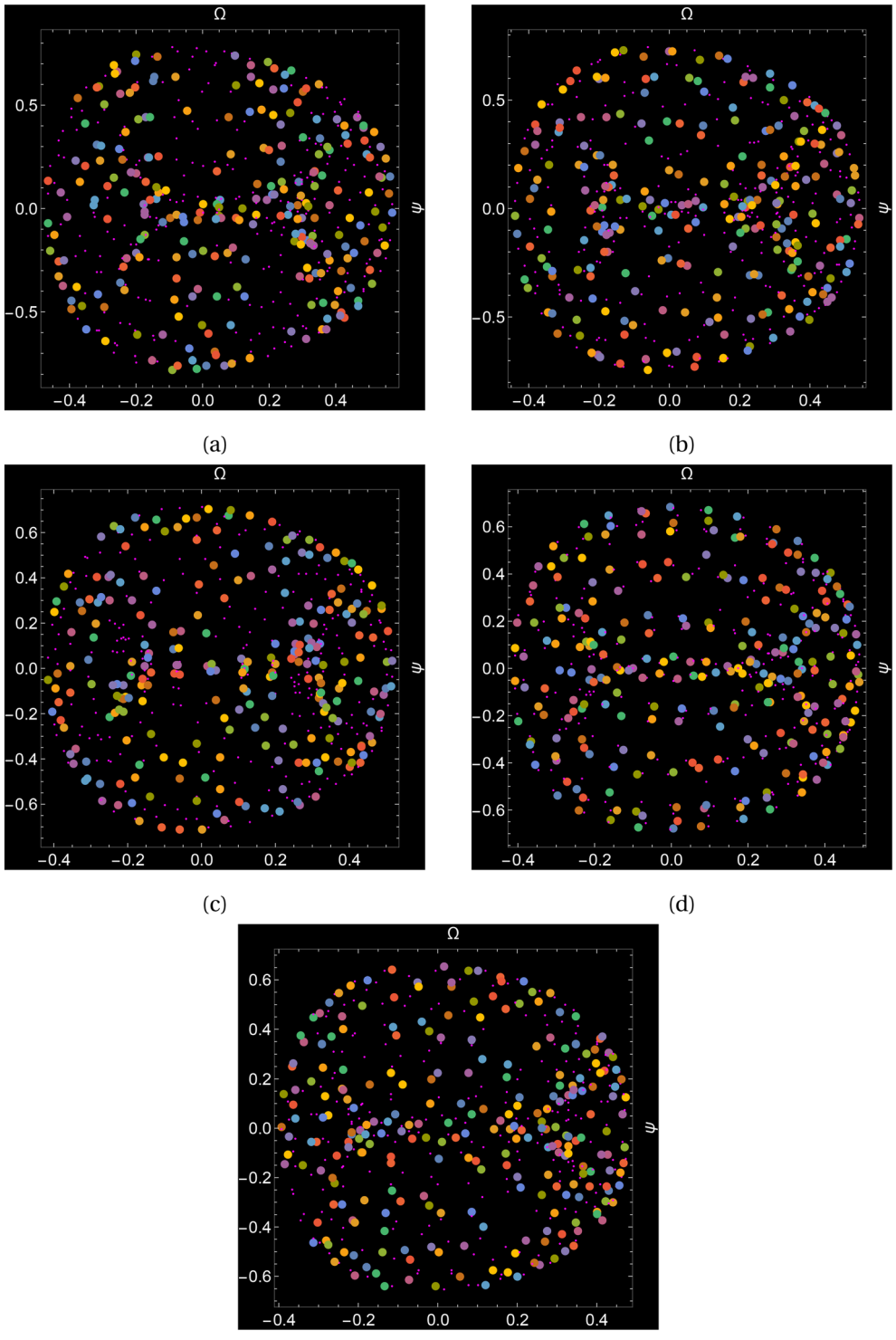


Fig. 12. Poincaré maps of the perturbed system (5.1) using the values $a = i\sqrt{3}, b = i\sqrt{3}, c = i\sqrt{3}, d = 0$, $\lambda_1 = -1, \lambda_2 = -1, \lambda_3 = -1, \gamma = 0, w_1 = -1, w_2 = 1, \omega = 1.20$ and (**a**) $\delta = 3.20$, (**b**) $\delta = 3.40$, (**c**) $\delta = 3.60$, (**d**) $\delta = 3.80$, (**e**) $\delta = 4$ with the initial condition $(\psi(0), \Omega(0)) = (0.29, 0.13)$.

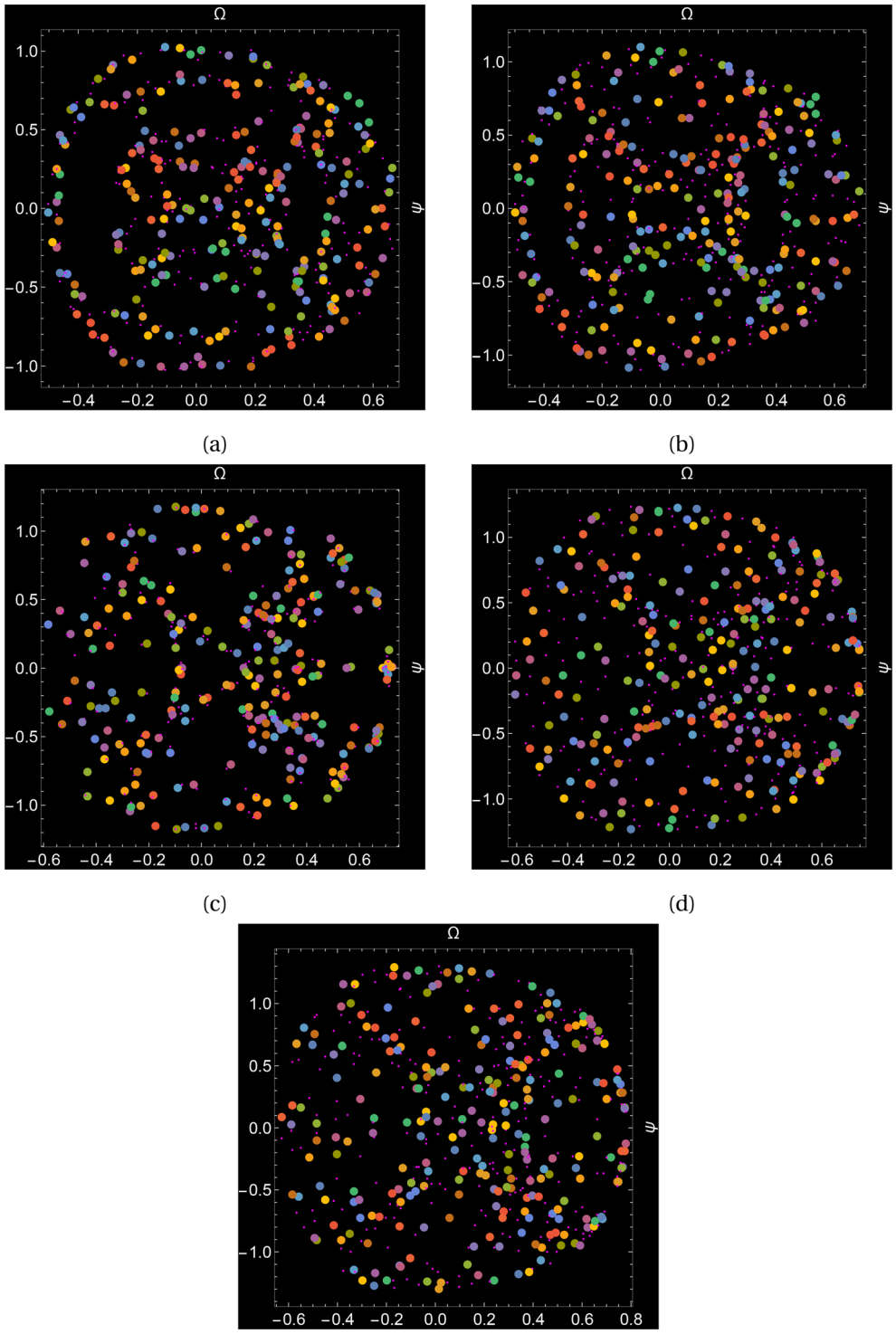


Fig. 13. Poincaré maps of the perturbed system (5.1) using the values $a = i\sqrt{3}, b = i\sqrt{3}, c = i\sqrt{3}, d = 0$, $\lambda_1 = -1, \lambda_2 = -1, \lambda_3 = -1, \gamma = 0, w_1 = -1, w_2 = 1, \delta = 3.60$ and (**a**) $\omega = 2.20$, (**b**) $\omega = 2.40$, (**c**) $\omega = 2.60$, (**d**) $\omega = 2.80$, (**e**) $\omega = 3.00$ with the initial condition $(\psi(0), \Omega(0)) = (0.29, 0.13)$.

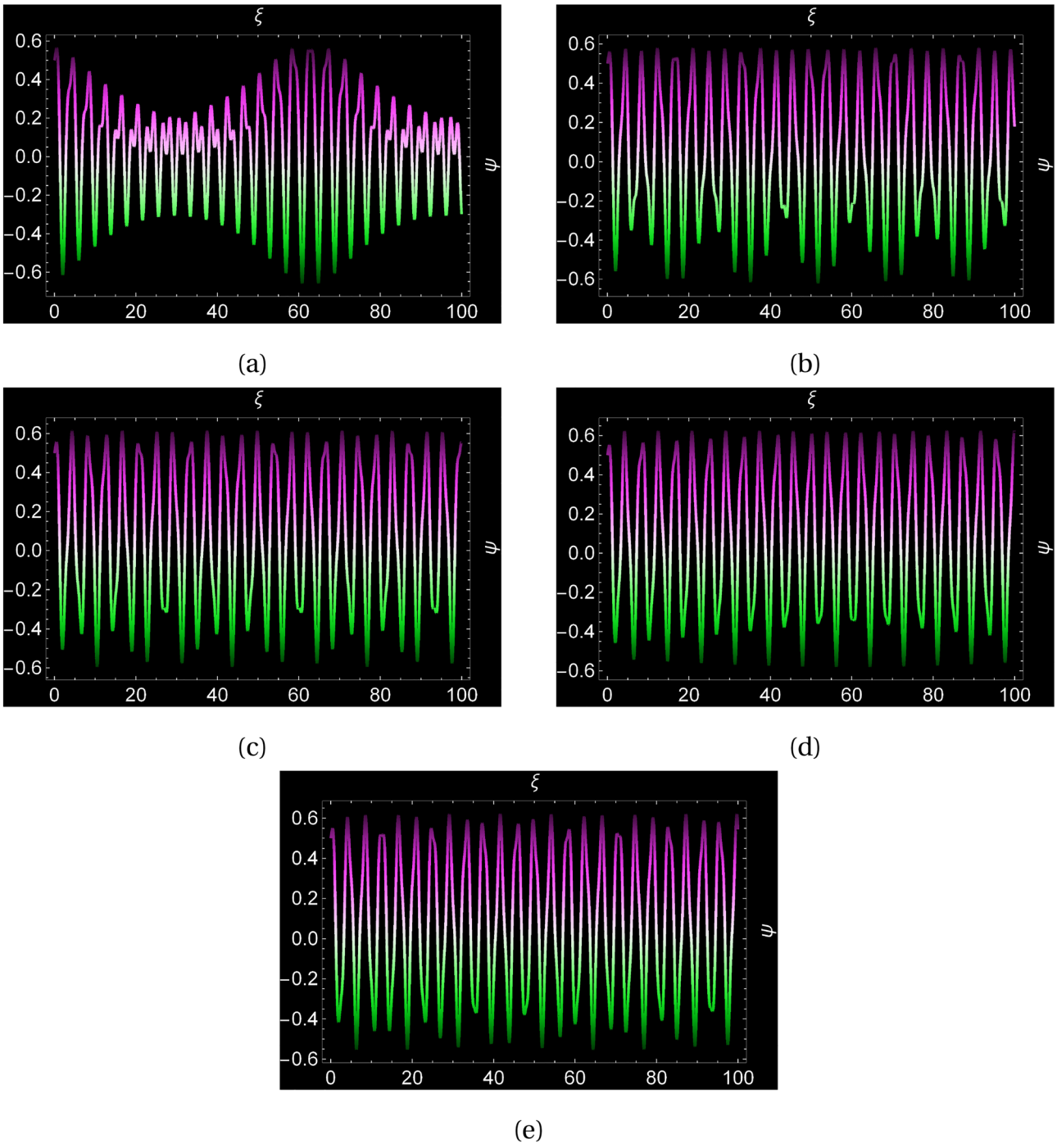


Fig. 14. Time series of the perturbed system (5.1) using the values $a = i\sqrt{2}, b = i\sqrt{2}, = i\sqrt{2}, d = 0$, $\lambda_1 = -2, \lambda_2 = -2, \lambda_3 = -1, \gamma = 0, w_1 = -2.5, w_2 = 1.5, f_0 = 1.25$, and (**a**) $\delta = 3.20$, (**b**) $\delta = 3.40$, (**c**) $\delta = 3.60$, (**d**) $\delta = 3.80$, (**e**) $\delta = 4.00$ with the initial condition $(\psi(0), \Omega(0)) = (0.5, 0.1)$.

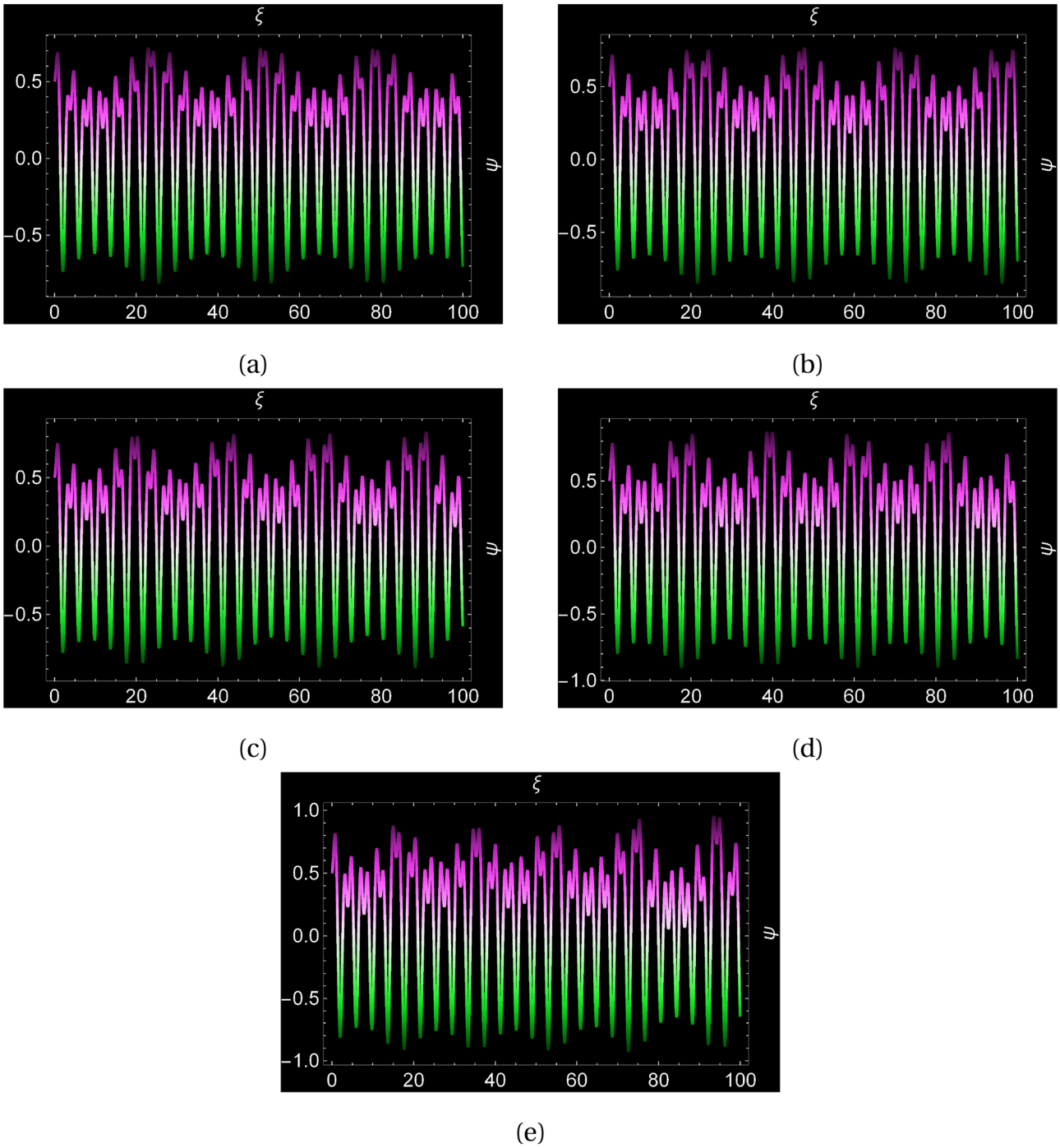


Fig. 15. Time series of the perturbed system (5.1) using the values $a = i\sqrt{2}, b = i\sqrt{2}, = i\sqrt{2}, d = 0$, $\lambda_1 = -2, \lambda_2 = -2, \lambda_3 = -1, \gamma = 0, w_1 = -2.5, w_2 = 1.5, \delta = 3.20$, and (**a**) $f_0 = 2.20$, (**b**) $f_0 = 2.40$, (**c**) $f_0 = 2.60$, (**d**) $f_0 = 2.80$, (**e**) $f_0 = 3.00$ with the initial condition $(\psi(0), \Omega(0)) = (0.5, 0.1)$.

Data availability

All data generated or analysed during this study are included in this published article.

Received: 4 August 2025; Accepted: 11 September 2025
Published online: 15 October 2025

References

1. Ramadan, M. E., Ahmed, H. M., Khalifa, A. S. & Ahmed, K. K. Invariant solitons and travelling-wave solutions to a higher-order nonlinear Schrödinger equation in an optical fiber with an improved tanh-function algorithm. *J. Appl. Anal. Comput.* **15**(6), 3270–3289 (2025).
2. Drazin, P. G. & Johnson, R. S. *Solitons: An Introduction* (Cambridge University Press, 1989).
3. Whitham, G. B. *Linear and Nonlinear Waves* (Wiley, 2011).
4. Asjad, M. I., Manzoor, M., Faridi, W. A. & Majid, S. Z. Precise invariant travelling wave soliton solutions of the Nizhnik–Novikov–Veselov equation with dynamic assessment. *Optik* **294**, 171438 (2023).
5. Majid, S. Z., Faridi, W. A., Asjad, M. I., Abd El-Rahman, M. & Eldin, S. M. Explicit soliton structure formation for the Riemann wave equation and a sensitive demonstration. *Fractal Fractional* **7**(2), 102 (2023).
6. Asjad, M. I., Majid, S. Z., Faridi, W. A. & Eldin, S. M. Sensitive analysis of soliton solutions of nonlinear Landau–Ginzburg–Higgs equation with generalized projective Riccati method. *AIMS Math.* **8**(5), 10210–10227 (2023).
7. Alqurashi, N. T., Manzoor, M., Majid, S. Z., Asjad, M. I. & Osman, M. S. Solitary waves pattern appear in tropical tropospheres and mid-latitudes of nonlinear Landau–Ginzburg–Higgs equation with chaotic analysis. *Results Phys.* **54**, 107116 (2023).
8. Ullah, N. et al. Novel waves structures for two nonlinear partial differential equations arising in the nonlinear optics via Sardar-subequation method. *Alex. Eng. J.* **71**, 105–113 (2023).
9. Ullah, N., Asjad, M. I., Almusawa, M. Y. & Eldin, S. M. Dynamics of nonlinear optics with different analytical approaches. *Fractal Fractional* **7**(2), 138 (2023).
10. Beenish, Samreen, M. Analytical solutions and dynamical insights of the modified Benjamin–Bona–Mahony equation with applications in nonlinear optics. *J. Appl. Math. Comput.*, 1–25 (2025).
11. Beenish, Asim, M., Boulaaras, S. & Rahman, M. U. Dynamical behaviour and solutions in the fractional Gross-Pitaevskii model. *Math. Comput. Model. Dyn. Syst.***31**(1), 2529190 (2025).
12. Beenish, & Samreen, M. Bifurcation, Multistability, and Soliton Dynamics in the Stochastic Potential Korteweg-de Vries Equation. *Int. J. Theor. Phys.* **64**(5), 1–22 (2025).
13. Khalifa, A. S., Ahmed, H. M. & Ahmed, K. K. Construction of exact solutions for a higher-order stochastic modified Gerdjikov–Ivanov model using the IMETF method. *Physica Scripta* (2024).
14. Singh, S. & Saha Ray, S. Painlevé integrability and new soliton solutions for (2+ 1)-dimensional Bogoyavlensky-Konopelchenko equation and generalized Bogoyavlensky-Konopelchenko equation with variable coefficients in fluid mechanics. *Int. J. Mod. Phys. B* **37**(14), 2350131 (2023).
15. Ray, S. S. On conservation laws by Lie symmetry analysis for (2+ 1)-dimensional Bogoyavlensky-Konopelchenko equation in wave propagation. *Comput. Math. Appl.* **74**(6), 1158–1165 (2017).
16. Weiss, J., Tabor, M. & Carnevale, G. The Painlevé property for partial differential equations. *J. Math. Phys.* **24**(3), 522–526 (1983).
17. Guo, J., He, J., Li, M. & Mihalache, D. Multiple-order line rogue wave solutions of extended Kadomtsev-Petviashvili equation. *Math. Comput. Simul.* **180**, 251–257 (2021).
18. Adem, A. R. & Khalique, C. M. New exact solutions and conservation laws of a coupled Kadomtsev-Petviashvili system. *Comput. Fluids* **81**, 10–16 (2013).
19. Kadomtsev, B. B. & Petviashvili, V. I. On the stability of solitary waves in weakly dispersive media. *Soviet Physics Doklady* **15**(6), 539–541 (1970).
20. Kaur, L. & Wazwaz, A. M. Dynamical analysis of soliton solutions for space-time fractional Calogero-Degasperis and Sharma-Tasso-Olver equations. *Rom. Rep. Phys* **74**, 108 (2022).
21. Yuan, F. Deformed soliton and positon solutions for the (2+ 1)-dimensional nonlinear Schrödinger equation. *Rom. Rep. Phys* **74**, 121 (2022).
22. Wazwaz, A. M., Alhejaili, W. & El-Tantawy, S. A. New (3+ 1)-dimensional Painlevé integrable extensions of Mikhailov-Novikov-Wang equation: Variety of multiple soliton solutions. *Rom. J. Phys.* **67**, 115 (2022).
23. Şenol, M. & Ghanbari, B. Exploration of novel traveling wave solitons to the conformable (3+ 1)-dimensional Wazwaz-Kaur-Boussinesq equation. *Int. J. Theor. Phys.* **64**(6), 151 (2025).
24. Wang, M., He, G., Xu, T. & Li, N. Localized waves for modified Boussinesq equation and Mikhailov-Lenells equation based on Physics-informed neural networks and Miura transformation. *Chaos Solitons Fractals* **190**, 115764 (2025).
25. Chen, G., Fang, K., Sun, J., Liu, Z., Wang, P. & Jin, H. A two-layer Boussinesq-type wave model accelerated by graphics processing unit. *Physics of Fluids***37**(7) (2025).
26. Cheng, Y., Dong, C., Zheng, S. & Hu, W. Solving nonlinear Boussinesq equation of second-order time derivatives with physics-informed neural networks. *Commun. Theor. Phys.* **77**(10), 105001 (2025).
27. Ma, Y. L., Wazwaz, A. M. & Li, B. Q. Novel bifurcation solitons for an extended Kadomtsev-Petviashvili equation in fluids. *Phys. Lett. A* **413**, 127585 (2021).
28. Ma, Y. L., Wazwaz, A. M. & Li, B. Q. New extended Kadomtsev-Petviashvili equation: Multiple soliton solutions, breather, lump and interaction solutions. *Nonlinear Dyn.* **104**, 1581–1594 (2021).
29. Wazwaz, A.-M. Study of three integrable extensions of Kadomtsev-Petviashvili, Boussinesq, and Kadomtsev–Petviashvili–Boussinesq equations. *Romanian Rep. Phys.* **76**, 114 (2024).
30. Wazwaz, A.-M. Extensions of Kadomtsev–Petviashvili and Kadomtsev–Petviashvili–Boussinesq equations: Multiple solitons and lump wave solutions. Romanian Reports in Physics. Advance online publication (2025).
31. Tariq, M. M., Riaz, M. B., Kazmi, S. S. & Aziz-ur-Rehman, M. Unveiling chaos and stability in advection diffusion reaction systems via advanced dynamical and sensitivity analysis. *Sci. Rep.* **15**(1), 5513 (2025).
32. Tariq, M. M., Riaz, M. B., Kozubek, T. & Aziz-ur-Rehman, M. Exploring chaos and stability: Dynamic insights into the stochastic Davey-Stewartson system through advanced sensitivity analysis. *Model. Earth Syst. Environ.* **11**(2), 83 (2025).
33. Riaz, M. B., Tariq, M. M., Kazmi, S. S. & Aziz-ur-Rehman, M. Exploring Nonlinear Dynamics and Stability of Embedded Carbon Nanotubes in Mechanical Engineering. *Arch. Computat. Methods Eng.*, 1–27 (2025).
34. Tariq, M. M., Riaz, M. B., Aziz-ur-Rehman, M. & Dilawaiz. Unraveling the complexity of solitary waves in the Klein-Fock-Gordon equation: dynamical insights into bifurcation and Chaos analysis. *Modeling Earth Systems and Environment***11**(1), 51 (2025).
35. Kopçasız, B. Qualitative analysis and optical soliton solutions galore: Scrutinizing the (2+1)-dimensional complex modified Korteweg–de Vries system. *Nonlinear Dyn.* **112**(23), 21321–21341 (2024).
36. Beenish, Samreen, M. Exploring quasi-periodic behavior, bifurcation, and traveling wave solutions in the double-chain DNA model. *Chaos, Solitons & Fractals***192**, 116052 (2025).
37. Strogatz, S. H. *Nonlinear Dynamics and Chaos: With Applications to Physics, Biology, Chemistry, and Engineering* 2nd edn. (CRC Press, 2018).
38. Alligood, K. T., Sauer, T. D. & Yorke, J. A. *Chaos: An Introduction to Dynamical Systems* (Springer, 1997).

Author contributions

M. Ş.: Formal analysis, Conceptualization, Methodology, Software, Validation; B. K. & K. K. A.: Formal analysis, Data curation, Writing-Original draft preparation; E. S. & H. E.: Visualization, Investigation, Writing-Reviewing, and Editing. All authors read and approved the final manuscript.

Declarations

Competing interests
The authors declare no competing interests.

Ethical approval
The authors state that this research paper complies with ethical standards. This research paper does not involve either human participants or animals.

Additional information
Correspondence and requests for materials should be addressed to H.E.

Reprints and permissions information is available at www.nature.com/reprints.

Publisher's note Springer Nature remains neutral with regard to jurisdictional claims in published maps and institutional affiliations.

Open Access This article is licensed under a Creative Commons Attribution-NonCommercial-NoDerivatives 4.0 International License, which permits any non-commercial use, sharing, distribution and reproduction in any medium or format, as long as you give appropriate credit to the original author(s) and the source, provide a link to the Creative Commons licence, and indicate if you modified the licensed material. You do not have permission under this licence to share adapted material derived from this article or parts of it. The images or other third party material in this article are included in the article's Creative Commons licence, unless indicated otherwise in a credit line to the material. If material is not included in the article's Creative Commons licence and your intended use is not permitted by statutory regulation or exceeds the permitted use, you will need to obtain permission directly from the copyright holder. To view a copy of this licence, visit http://creativecommons.org/licenses/by-nc-nd/4.0/.

© The Author(s) 2025